

# Establishing the level of cylindrical rotation in Boxy/Peanut bulges

A. Molaeinezhad<sup>1\*</sup>, J. Falcón-Barroso<sup>2,3</sup>, I. Martínez-Valpuesta<sup>2,3</sup>, H.G. Khosroshahi<sup>1</sup>,  
M. Balcells<sup>2,4</sup>, and R.F. Peletier<sup>5</sup>

<sup>1</sup>*School of Astronomy, Institute for Research in Fundamental Sciences (IPM), PO Box 19395-5746 Tehran, Iran*

<sup>2</sup>*Instituto de Astrofísica de Canarias, E-38200, La Laguna, Spain*

<sup>3</sup>*Depto. Astrofísica, Universidad de La Laguna (ULL), E-38206 La Laguna, Tenerife, Spain*

<sup>4</sup>*Isaac Newton Group of Telescopes, Apartado 321, 38700 Santa Cruz de La Palma, Canary Islands, Spain*

<sup>5</sup>*Kapteyn Astronomical Institute, University of Groningen, Postbus 800, 9700 AV Groningen, the Netherlands*

Accepted 2015 November 16. Received 2015 November 05; in original form 2015 July 07

## ABSTRACT

We present SAURON integral-field observations of a sample of 12 mid to high-inclination disk galaxies, to unveil hidden bars on the basis of their kinematics, i.e., the correlation between velocity and  $h_3$  profiles, and to establish their degree of cylindrical rotation. For the latter, we introduce a method to quantify cylindrical rotation that is robust against inner disk components. We confirm high-levels of cylindrical rotation in boxy/peanut bulges, but also observe this feature in a few galaxies with rounder bulges. We suggest that these are also barred galaxies with end-on orientations. Re-analysing published data for our own Galaxy using this new method, we determine that the Milky Way bulge is cylindrically rotating at the same level as the strongest barred galaxy in our sample. Finally, we use self-consistent three-dimensional  $N$ -body simulations of bar-unstable disks to study the dependence of cylindrical rotation on the bar's orientation and host galaxy inclination.

**Key words:** galaxies: bulges galaxies: kinematics and dynamics galaxies: spiral - Galaxy: bulge - Galaxy: kinematics and dynamics.

## 1 INTRODUCTION

Barred galaxies represent a considerable fraction of the entire disk galaxy population (e.g. Eskridge et al. 2000; Knapen et al. 2000; Whyte et al. 2002; Grosbøl et al. 2004; Marinova & Jogee 2007). In edge-on or highly inclined systems, bars are most easily recognised by boxy and peanut-shapes, and sometimes X-shape morphology formed by the stellar material above the disk plane (e.g. Kuijken & Merrifield 1995; Bureau & Freeman 1999). Bars in this configuration are usually termed Boxy/Peanut bulges (hereafter BP bulges).

$N$ -body simulations of bar-unstable disks indicate that BP bulges could form out of disc material, via the vertical buckling instability of the bar (e.g. Raha et al. 1991; Martínez-Valpuesta & Shlosman 2004; Martínez-Valpuesta et al. 2006). However, including gas in the simulations may suppress buckling and as a result, the peanut can form without a vertical buckling phase (e.g. Berentzen et al. 1998, 2007; Villa-Vargas et al. 2010; Debattista et al. 2006; Wozniak & Michel-Dansac 2009). (For a general review of this subject, see Athanassoula 2015).

Finding observational evidence to establish a link between bars and BP shape is sometimes complicated. The vertically thickened regions of bars are not observable photometrically if the

galaxy is not inclined enough (e.g. Athanassoula & Beaton 2006; Erwin & Debattista 2013), while the presence of a bar is generally apparent, on the basis of photometry alone, if the galaxy is viewed in a more face-on orientation. In fact, the best viewing angles, giving information on both the BP and bar, are intermediate inclination, but close to edge-on (see Athanassoula 2015, and the references therein). BP bulges are best seen when the bar is at an intermediate angle or perpendicular to the line-of-sight. Bars oriented exactly parallel to the line-of-sight appear almost spherical and thus difficult to identify (Bureau et al. 2004; Athanassoula 2015).

BP bulges specifically and bars in general produce distinct kinematic features that can be easily detected in galaxies. Bureau & Athanassoula (2005) established, using  $N$ -body simulations, a number of kinematic properties in bars of different strength and orientations in highly-inclined systems. They are most noticeable in the major-axis rotation and velocity dispersion profiles (e.g. “double-hump” rotation curves, velocity dispersion profiles with a plateau at moderate radii), but they also leave more subtle signatures in the higher order moments of the Gauss-Hermite series (e.g. a positive correlation between the velocity and the  $h_3$  over the length of the bar). These features have been confirmed in several observational studies (e.g. Pence 1981; Kormendy 1983; Bettoni & Galletta 1997; Emsellem et al. 2001; Márquez et al. 2003; Pérez et al. 2009; Williams et al. 2011). While being a powerful indicator for the presence of bars, the  $V - h_3$  correlation has hardly been used for this purpose in observational

\* Email: molaei@ipm.ir

studies (e.g. Chung & Bureau 2004). All these diagnostics have been recently expanded (Iannuzzi & Athanassoula 2015) to be applied to the wealth of data from existing or upcoming integral-field spectroscopic surveys (e.g. ATLAS3D, Cappellari et al. 2011; CALIFA, Sánchez et al. 2012; SaMI, Croom et al. 2012; MaNGA, Bundy et al. 2015).

Cylindrical rotation (Kormendy & Illingworth 1982) is another major kinematic characteristic feature of BP bulges (e.g. Kormendy & Illingworth 1982; Bureau & Freeman 1999; Falcón-Barroso et al. 2006). In such systems, the mean stellar rotation speed is almost constant with height above the disk plane. This feature is well described by the formation and evolution scenarios of BP bulges through the vertical buckling instability of the bar (Combes & Sanders 1981; Martínez-Valpuesta & Shlosman 2004) and, subsequently, many  $N$ -body simulations of barred galaxies (e.g. Combes et al. 1990; Sellwood & Wilkinson 1993; Athanassoula & Misiriotis 2002; Bureau & Athanassoula 2005; Saha et al. 2012; Martínez-Valpuesta & Gerhard 2013; Saha et al. 2013) present such feature in the velocity maps. Williams et al. (2011) studied the stellar kinematics and populations of BP bulges in a relatively small sample of five edge-on galaxies using long slit spectroscopy. Their main conclusion is that the degree of cylindrical rotation varies significantly among BP bulges, as do the properties of their stellar populations. That study was the first to challenge the simple picture of BP bulges and claimed that they do not form a homogeneous class of objects. Saha et al. (2012) investigated the interaction of a bar and a low-mass classical bulge via a high spatial resolution  $N$ -body simulation of a galaxy consisting of a live disc, a bulge and dark matter halo. They followed the evolution of the kinematics of the small classical bulge. In their study, they show that the classical bulge could acquire cylindrical rotation by exchanging angular momentum with the surrounding bar. Later on, Saha & Gerhard (2013) introduced a criterion to quantify deviations from pure cylindrical rotation in edge-on disk galaxies and use this quantity to show that the level of cylindrical rotation in BP bulges is time-dependent.

This paper presents the first results of our analysis of the properties of BP bulges in nearby galaxies. Here we will focus on the stellar kinematics of a sample of 12 intermediate inclined disk galaxies ( $i > 60^\circ$ ) to unveil the presence of bars and to quantify the level of cylindrical rotation in these systems. In future papers we will connect these features with the stellar population properties of these galaxies. The paper is structured as follows. In Section 2 we introduce our sample and the photometric and spectroscopic datasets used for this work. Section 3 we study the signature of the bar in our 2D kinematics maps and methods to unveil the hidden or end-on bars based on  $N$ -body simulations results. Section 4 is devoted to discuss the signature of cylindrical rotation and methods to describe it in BP bulges. In Section 5, we focus on the determination of the cylindrical rotation in the Milky Way (MW) bulge. Section 6 discusses the possible correlation between bars, BP bulges and level of cylindrical rotation. We summarize our results and draw our conclusions in Section 7.

## 2 SAMPLE & IFU OBSERVATIONS

### 2.1 Sample Selection & Properties

Our sample for this study comprises 12 intermediate inclined galaxies ( $i > 60^\circ$ ) selected from the well-characterised sample of Balcells & Peletier (1994), of inclined early-type spiral galaxies

and S0's.<sup>1</sup> This preferred orientation allows us to use the relatively little obscured side of the bulge. The sample was complemented with NGC 0678, that followed the same selection criteria and had similar SAURON integral-field spectroscopic observations.

The SAURON data for the galaxies in our sample have not been published before, apart from NGC 5475 and NGC 5689 (Falcón-Barroso et al. 2006) and NGC 7332 (Falcón-Barroso et al. 2004). For these 3 galaxies, the data published here is the same as was presented before. However, in these papers, the issue of cylindrical rotation was not addressed. The other 9 galaxies, although observed with SAURON, are not part of the SAURON sample, nor of the sample of late-type spirals of Ganda et al. (2006). The sample was observed independently, as part of a project to study the vertical kinematics and population structure of bulges. The observed field of view and spatial resolution is well matched to the sizes of the bulges. The  $S/N$  of the data is considerably higher than that of the ATLAS3D survey (Cappellari et al. 2011), on which we will elaborate in the second paper of this series. Another advantage of this sample is that the extinction properties have been well-studied (Peletier et al. 1999). We present all the kinematic maps and new diagnostics developed in this paper in Appendix A.

These objects have been the subject of several studies on galactic bulges by the original authors (e.g. Peletier & Balcells 1996, 1997; Peletier et al. 1999; Falcón-Barroso et al. 2002; Balcells et al. 2003a,b; Falcón-Barroso et al. 2003a,b; Balcells et al. 2007a,b) and have extensive ground-based and *Hubble Space Telescope* optical observations as well as NIR photometry.

It is worth noting that in this study, we do not label our bulges as classical or pseudobulges or bars, trying to make the analysis independent of the photometric appearance of the bulges. Through this study, the 'bulge' of a galaxy is referred to the excess of light that is above the main disk. On the other hand, it is our aim to do a study that is as independent as possible from photometric studies in the past, as obviously by performing a decomposition into various types of bulges, the results will be severely biased. This way of defining the bulge might bias against certain type of bulges like as pseudo bulges. In §3 we will briefly discuss the masking effect of a classical bulge on the kinematics signatures of barred systems.

### 2.2 Morphology Analysis

The overall shape of the non-axisymmetric component in highly inclined galaxies is not directly visible in the images, but becoming clear in unsharp masking or residual images in decompositions. Figure 2 (second and third panels) shows the isophotes and unsharp masks of the  $K$ -band images for all 12 galaxies in our sample. Our  $K$ -band images were obtained with the UK infrared telescope (UKIRT), using the IRCAM3 Camera (Peletier & Balcells 1997). For NGC 0678 we have used  $i$ -band Sloan Digital Sky survey DR10 data (Ahn et al. 2014). The images after unsharp masking (median filtering) show the high frequency features of the images and an X-shaped structure is clearly visible for 6 galaxies in our sample (NGC 0678, NGC 5422, NGC 5689, NGC 5746, NGC 5965 and NGC 7332). The lower panels of Figure 2 presents the isophotes of the  $K$ -band image, after subtracting an exponential disk from the observed image. For this purpose, we used GALFIT (Peng et al.

<sup>1</sup> The optical and near-infrared (NIR) surface brightness and colour profiles of galaxies in the original sample of are available in the web page <http://www.astro.rug.nl/~peletier/www/newast.html>

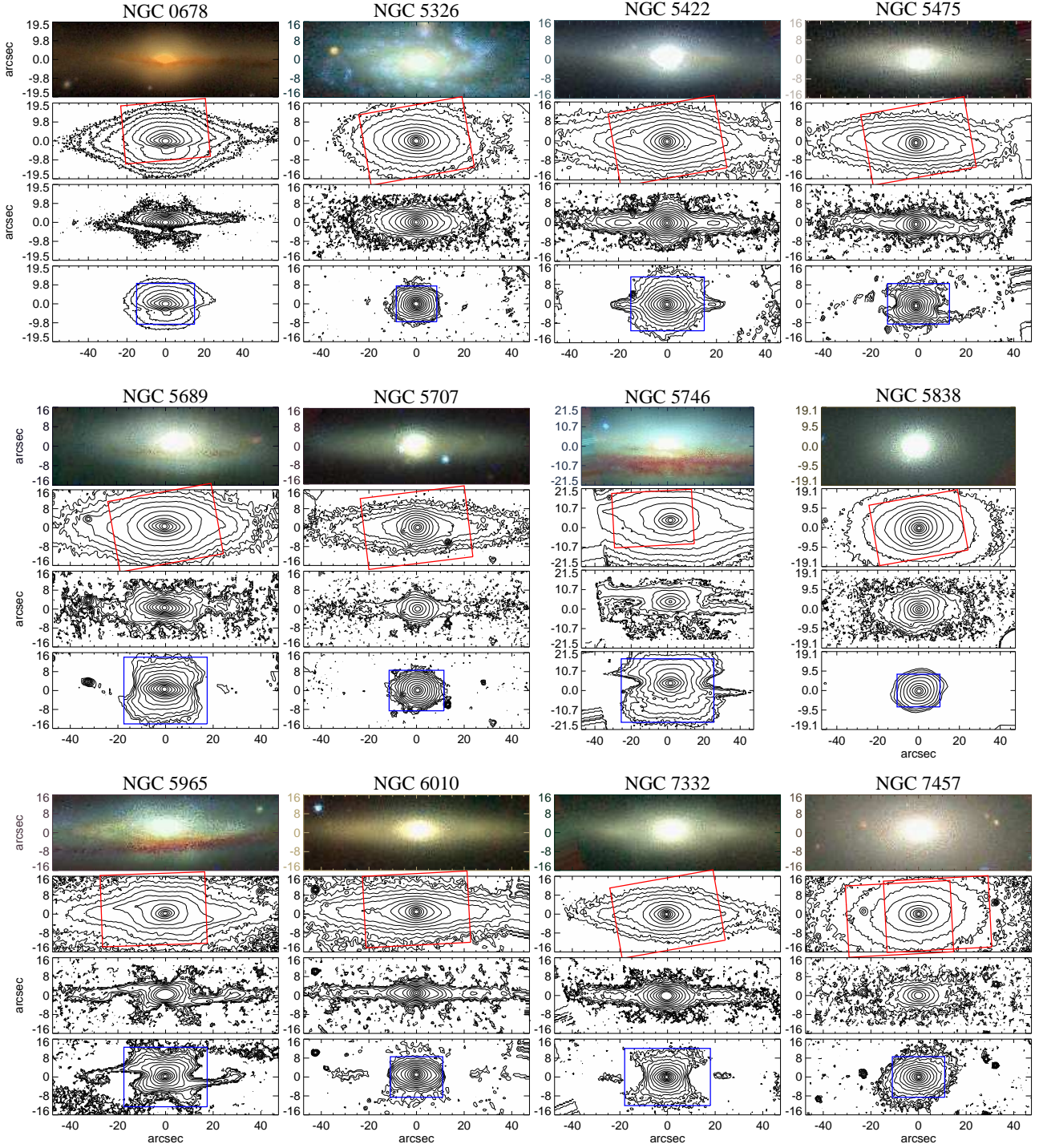


**Figure 2.** *U-R-K* composite images, Isophotes and unsharp masks for all 12 galaxies in our sample. For each galaxy, First panel: The *U-R-K* composite image, from Peletier & Balcells (1997). *U*- and *R*-band images were obtained with the Prime Focus camera of the Isaac Newton telescope and *K*-band images were taken at the UK infrared telescope (UKIRT), using the IRCAM3 Camera. For NGC0678 we have used Sloan Digital Sky survey DR10 data. Second panel: Isophotes of the *K*-band images. The SAURON final pointing is shown on top of this panel. Third panel: Unsharp masked *K*-band image. The unsharp masking technique allows us to highlight the structure of the galaxy in more details, for instance, the X-shape bulge is clearly visible for 6 galaxies in our sample (NGC 0678, NGC 5422, NGC 5689, NGC 5746, NGC 5965 and NGC 7332). Fourth Panel: Isophotes of the *K*-band image, after subtracting an exponential disk from the observed image. We have used the disk-subtracted images together with the unsharp masked galaxy images (third panel) to have a rough estimation of bulge size in the  $(x, z)$  space. This analysis bulge window is shown as a blue rectangle on top this panel.



2002) to find the best exponential disk model while the central regions (0.5 kpc) of galaxies are masked to avoid any possible influence of bright central components. As our goal was to model the outer disks, we found such masking approach more useful than putting any constraints on the fitting parameters, while the radius of this masked region is large enough to avoid large bulges from affecting the disk fit. The fitting process has been repeated using different initial parameters to obtain the best disk model. In the fourth panel of Figure 2, for each galaxy, we show the residual image, obtained after subtracting the disk from the original image.

It is obvious that ignoring the bar component from the fitting process will introduce a bias in the fitted parameters of the bulge and the disk. As also stated in Gadotti (2008) both bulge and disk components will try to accommodate the light from the ignored bar. The resulting disks will have a steeper luminosity profile, and a stronger effect will be seen in the bulge which will acquire a larger effective radius and luminosity fractions. This works in favor of our goal which is not to miss any possible bulge contribution. Again we stress that the purpose of this exercise is to obtain a rough estimation for the bulge analysis window by modeling out the exponential disk. We use the term "photometric bulge" to indicate that we do not discriminate between different types of bulges in this study.

Evaluation of the photometric bulge analysis radius in  $x$  (or  $z$ ) direction has been performed by stacking the residual images (single exponential disk subtracted), along the minor (or major) axis and evaluating the radius, at which 90% of the galaxy light is concentrated within that radius. The 90% was preferred to lower typical values such as 75 or 50% just to make sure that the whole bulge area is covered during our analysis. However, selecting different thresholds (50, 75 or 90%) for the bulge radius does not impose any major difference, as the brightness profile of the bulge is much steeper than that of the disk. Comparing the third and fourth panel of Figure 2 for each galaxies demonstrates good agreement between this approach to evaluate the bulge analysis window and that one could obtain using unsharp masked image.

Clearly, the radial extent parameters  $x_B$  and  $z_B$  shrink if a luminous spheroidal component exists in the center of a box-peanut light distribution. This is acceptable to us, given that we are after the kinematics of everything, excluding the exponential disk. Any possible bias in our results due to our proposed method to evaluate the bulge analysis windows will be discussed later.

In our study, we are interested in determining the level of cylindrical rotation of these bulges and thus it is important how many of them are BP bulges and how many are largely spherical. It is widely accepted that fourth order Fourier coefficients ( $c_4$ ) of an ellipse-fit extraction can be used to measure the level of boxiness or diskiness of different structural components in galaxies. This method has been used by many authors to quantify the degree of boxiness in bulges (e.g. Combes et al. 1990; Shaw et al. 1993; Lütticke 1996; Merrifield & Kuijken 1999). We attempted to carry out this type of analysis in our sample, but we were not successful to obtain robust results. Difficulties arose due to the amount of dust present in many of these galaxies. Being close to edge-on, dust in the main disk is very prominent and thus complicates the extraction of reliable ellipse-fit profiles. The particular orientation of our galaxies, also causes that different structures with very distinct  $c_4$  signal (e.g. boxy bulges and inner disks) overlap in projection and produce an ambiguous  $c_4$  value. Such inconsistencies between the visual inspections and the results of isophotal analysis have been discussed in the literature (e.g. Lütticke et al. 2000). As they argued, a major disadvantage of using isophotal analysis is not only the presence of dust, but the influence of the masked stars in the foreground, pres-

ence of non-axisymmetric structure like flat bars, thick disk, inner disks and the extreme nature of BP isophotal distortions for the ellipse fitting.

In order to overcome this issue, and similar to Lütticke (1996), we evaluate the level of boxiness of bulges in our sample by visually inspecting residual images after subtracting an exponential disk model to the galaxies. As we mentioned earlier, the result of this exercise on our  $K$ -band images of our sample is presented in Figure 2.

Our analysis of the residual images in addition to the unsharp masked images suggest that 6 galaxies host prominent BP bulges (NGC 0678, NGC 5422, NGC 5689, NGC 5746, NGC 5965 and NGC 7332), while the rest harbour relatively spherical bulges or there is no clear sign of X-shape structure in the related unsharp masked images. Our morphological classification of these bulges is consistent with the previous studies (Lütticke et al. 2000; Chung & Bureau 2004; Williams et al. 2011). The basic photometric properties of all 12 galaxies in our sample are summarised in Table 1.

### 2.3 Integral-field observations and data reduction

Spectroscopic observations were carried out between October 1999 and 2011 with the SAURON integral-field spectrograph (Bacon et al. 2001) attached to the 4.2-m William Herschel Telescope (WHT) of the Observatorio del Roque de los Muchachos at La Palma, Spain. We used the low spatial resolution mode of SAURON which gives a  $33'' \times 41''$  field-of-view (FoV), with a spatial sampling of  $0''.94 \times 0''.94$ . This setup produces 1431 spectra per pointing over the SAURON FoV. Additionally, a dedicated set of 146 lenses provide simultaneous sky spectra  $1''.9$  away from the main field. The spectral resolution delivered by the instrument is  $\sim 4.2 \text{ \AA}$  (FWHM) and covers the narrow spectral range 4800–5380  $\text{\AA}$ . This wavelength range includes a number of important stellar absorption features (e.g.  $H\beta$ , Fe5015, Mg $b$ , Fe5270) and also potential emission lines ( $H\beta\lambda 4861$ ,  $[O III]\lambda\lambda 4959, 5007$ ,  $[N I]\lambda\lambda 5198, 5200$ ).

For each galaxy, typically four overlapping exposures of 1800 s were typically obtained. An offset of a few arcseconds was introduced between exposures to avoid bad CCD regions. Single pointings were required to cover the bulge dominated region. We followed the procedures described in (Bacon et al. 2001) for the data reduction of the data using the specifically designed XSAURON software developed at CRAL. For each galaxy, the sky level was measured using the dedicated sky lenses and subtracted from the target spectra. Arc lamp exposures were taken before and after each target frame for wavelength calibration. Tungsten lamp exposures were also taken at the beginning and end of each night in order to build the mask necessary to extract the data from the CCD frames. Flux standard stars were observed during each observing run for calibration purposes. The individually extracted and flux calibrated datacubes were finally merged by truncating the wavelength domain to a common range and spatially resampling the spectra to a common squared grid. The dithering of individual exposures enabled us to sample the merged datacube onto  $0''.8 \times 0''.8$  pixels.

In order to ensure the measurement of reliable stellar kinematics, we spatially binned our final datacubes using the Voronoi 2D binning algorithm of Cappellari & Copin (2003), creating compact bins with a minimum signal-to-noise ratio ( $S/N$ ) of  $\sim 40$  per spectral resolution element. Most spectra in the central regions, however, have  $S/N$  in excess of 40, and so remain un-binned. The stellar kinematic maps used in this paper (velocity  $[V]$ , velocity dispersion  $[\sigma]$ ,  $h_3$  and  $h_4$ ) were obtained following the same pro-

**Table 1.** Basic properties of our sample of galaxies

Galaxy	$V_{LG}$ ( $km\,s^{-1}$ )	Scale ( $kpc''$ )	B/D	Inclination ( $deg$ )	Type (RC3)	Type (Buta + 2015)	PA ( $deg$ )	$x_B$ ( $arcsec$ )	$z_B$ ( $arcsec$ )
(1)	(2)	(3)	(4)	(5)	(6)	(7)	(8)	(9)	(10)
NGC 0678	3015	0.19	-	82	<i>SB(s)b sp</i>	<i>SAB(s,nd)a sp</i>	9	15.0	10.5
NGC 5326	2596	0.17	0.73	65	<i>SAa?</i>	<i>E(d)5/S0 sp</i>	-138	8.5	7.5
NGC 5422	1977	0.13	1.28	90(90)	<i>S0 sp</i>	<i>SAB<sub>a</sub>0° sp/E(d)8</i>	64	15.0	11.0
NGC 5475	1815	0.12	0.14	78(79)	<i>SA? sp</i>	-	-101	13.0	8.5
NGC 5689	2295	0.15	0.89	81	<i>SB(s)0/a</i>	<i>(R'L)SAB : (r'l,nd)0<sup>+</sup> sp</i>	-5	17.5	14.0
NGC 5707	2358	0.15	0.42	80	<i>Sab? sp</i>	<i>SA0° sp</i>	-59	11.5	8.5
NGC 5746	1680	0.12	0.68	81	<i>SAB(rs)b? sp</i>	<i>(R')SB<sub>x</sub>(r,nd)0/a sp</i>	-99	25.5	17.5
NGC 5838	1316	0.09	0.71	72	<i>SA0<sup>-</sup></i>	-	134	10.5	8.0
NGC 5965	3603	0.23	0.53	80	<i>Sb</i>	-	-38	17.5	12.5
NGC 6010	2036	0.14	0.27	84(90)	<i>S0/a? sp</i>	<i>SA(l)0° sp</i>	12	11.0	8.5
NGC 7332	1481	0.08	0.41	81(84)	<i>S0 pec sp</i>	-	-114	18.0	12.0
NGC 7457	1134	0.06	10.0	70(74)	<i>SA0<sup>-</sup>(rs)?</i>	-	35	11.0	8.5

NOTES: (1) Galaxy name. (2) Recession velocity of each galaxy in  $km/s$ , corrected to the Local Group (Karachentsev and Makarov 1996). (3) Spatial scale in  $kpc/arcsec$  at the galaxy distance, assuming  $H_0 = 70\,km/s/Mpc$ . (4) Bulge-to-Disk luminosity ratio from a bulge-disk decomposition in  $R$ -band (Peletier & Balcells 1997), following Kent (1984) method. (5) Galaxy inclination evaluated from disk ellipticity in  $R$ -band from Peletier & Balcells (1997), corrected for finite disk thickness. Inclinations evaluated from the best fitting mass-follow-light JAM models (Cappellari et al. 2013) are also mentioned, if available. (6) Morphological type from the Third Reference Catalog of Bright Galaxies (de Vaucouleurs et al. 1991, hereafter RC3). (7) Morphological classification by Buta et al. (2015) from the Spitzer Survey of Stellar Structure in Galaxies ( $S^4G$ ). (8) The position angle (N–E) of the dust free minor axis. (9) and (10) Analysis window of the bulge along the major and minor axis respectively. Refer to text for more details.

cedure outlined in Falcón-Barroso et al. (2006) using the penalised pixel fitting (pPXF) routine by Cappellari & Emsellem (2004) and the MILES stellar population models as templates (Vazdekis et al. 2010; Falcón-Barroso et al. 2011).

### 3 UNVEILING HIDDEN BARS WITH KINEMATICS

$N$ -body simulations of bar-unstable disks have established that BP bulges are simply the thick part of bars extending above the galaxy disk. Our ability to detect bars via photometry depends on the viewing angle of the bar and galaxy inclination, as bars oriented parallel to the line of sight could remain undetected. An alternative to the photometric observations is the use of the stellar kinematics. As mentioned earlier, self-consistent, three-dimensional  $N$ -body simulations of bar-unstable disks (see Bureau & Athanassoula 2005, for more details) suggest a number of the major-axis stellar kinematic features that can be used as bar diagnostics: (1) a “double-hump” rotation curve; (2) a broad central velocity dispersion peak with a shoulder or plateau (and possibly a secondary maximum) at moderate radii; and (3) an  $h_3$  profile correlated with  $V$  over the projected bar length. They also showed that a local central velocity dispersion minimum can also be present for strong bars seen approximately end-on.

Following this work, Chung & Bureau (2004) presented long-slit stellar kinematic profiles of 30 edge-on spiral galaxies, mostly with BP bulges. The one-dimensional kinematic profiles of most galaxies in their sample were consistent with those predicted from  $N$ -body simulations. Nevertheless, they also pointed out a number of differences, which are most likely due to the absence of a dissipative component in such simulations (see Friedli & Benz 1993; Wozniak et al. 2003). They found that in 60% of galaxies in their sample  $h_3$  is strongly anti-correlated with  $V$  in the very central regions. They related this feature to the presence of cold and dense decoupled central stellar disks, and argued this inner disk formed out of gas accumulated by the bar at the centre through in-

flow. Their results, however, confirmed that the positive correlation of  $V$  and  $h_3$  can also be considered a reliable indicator of bars.

Recently, Iannuzzi & Athanassoula (2015) studied the imprints of boxy/peanut structures on the 2D line-of-sight kinematics of simulated disk galaxies. They recover the results of Bureau & Athanassoula (2005) as well as their dependence on the strength of the boxy/peanut and its position angle and various projection effects. To this, they also add the peanut related signatures in the form of elongated wings of large  $h_3$  values and X-shaped regions of deep  $h_4$  minima, roughly in an area covering the peanut (see Iannuzzi & Athanassoula 2015; Athanassoula 2015, for more details).

We have taken advantage of this diagnostic tools to unveil the presence of hidden bars in our sample. In this section we will focus in particular on the  $V$  and  $h_3$  correlation. We have used the correlation between  $V$  and  $h_3$  to unveil the presence of hidden bars in our sample. For this purpose, we have extracted profiles of these two parameters on pseudo-slits parallel to the major axis, at various heights from the major axis. These profiles are extracted only on the clean (i.e., dust-free) side of our galaxies to avoid issues with dust extinction. Prominent cases with clear dust disks are NGC 5746 and NGC 5965. We have then determined the linear Pearson correlation coefficient (e.g. Taylor 1996) between  $V$  and  $h_3$  for each pseudo-slit. The resulting correlation values are shown in Figure 3 for the entire sample. The error bar for each point represents the standard error of the correlation coefficient (Ghosh 1966). In these plots, a value of -1 indicates a negative correlation and +1 means positive correlation. Light purple shaded areas mark regions closer to the disk plane, where signs of an anti-correlation due to the presence of inner disks are expected. The intermediate regions mark the bulge/bar dominated regions where, if present, we expect to measure a positive correlation between  $V$  and  $h_3$ .

The inspection of these profiles reveals that most (8 out of 12) galaxies in our sample display positive correlation in the areas above the mid-plane. This (positive) correlation is most visible in those systems with BP bulges. Our data therefore confirms pre-

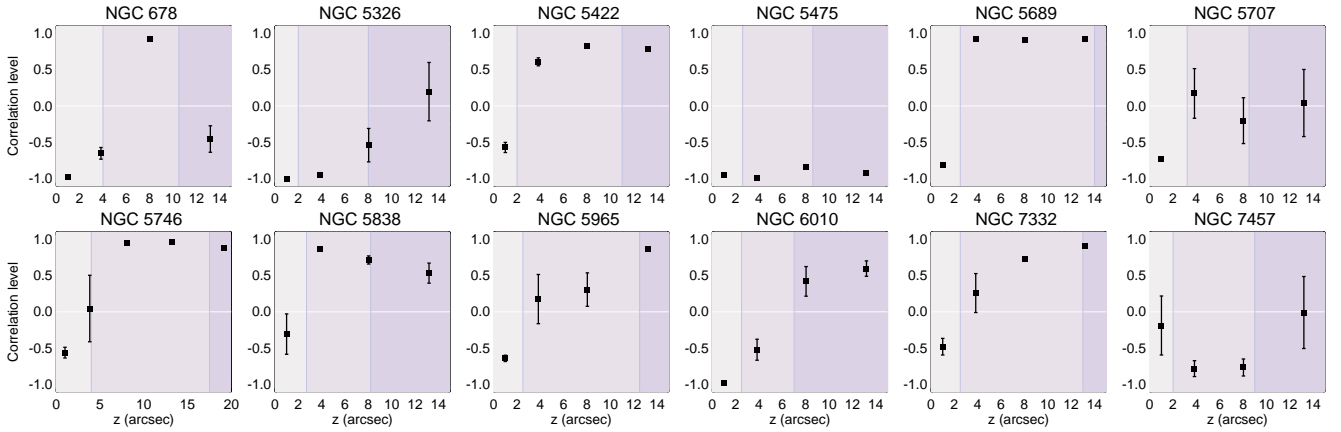


**Figure 3.** The  $V - h_3$  correlation profiles for all galaxies in our sample. These profiles show the level of correlation of  $V$  and  $h_3$  within the bulge zone in pseudo-slits parallel to the major axis of the galaxies at different heights ( $z$ ) from the disk plane. These measurements have been performed on the dust-free side of the galaxies. Negative values indicate negative correlation, while values closer to +1 mean stronger positive correlation. Different shaded regions mark the disk plane, the bulge/bar dominated parts and the regions beyond  $z_B$ .

vious claims that positive  $V - h_3$  correlation is strongly associated with bars. That several galaxies show positive  $V - h_3$  correlation well outside the region of the photometric bulge is an indicator that photometric decomposition does not clearly separate regions with distinct bulge and disk dynamics. If regions of positive  $V - h_3$  correlation are dynamically set by the action of bars, our result suggests that, at least in high-inclination views, such regions extend out beyond the photometric bulge and merge smoothly with the outer exponential disk.

Moreover, 10 of 12 galaxies in this sample, clearly exhibit a strong anti-correlation ( $< -0.5$ ) of  $h_3$  and  $V$  in the central regions, similar to what is observed by (e.g. Chung & Bureau 2004; Falcón-Barroso et al. 2006) in barred galaxies, and associated to rotating inner structures. In our sample, all galaxies with BP bulges show this feature in their central regions.

As mentioned earlier, Iannuzzi & Athanassoula (2015) investigated the dependencies between the various projection effects and bar strength on the kinematic diagnostics of barred system. They show that for stronger BPs, the kinematic maps change considerably from the side-on to the end-on projection in both the amplitude of the moments and their morphology and involve interesting features offset from the major axis. Specifically, the  $V - h_3$  correlation blobs become larger and extend farther out from the centre, while for moderate BPs the changes are considerably reduced and are essentially in the magnitude of the moments. Considering this issue, we can study a peculiar galaxy in this analysis: NGC 5838. Despite having a nearly spherical bulge, NGC 5838 displays a high level of correlation between  $h_3$  and  $V$  over the bulge region. NGC 5838 shows also properties akin of barred galaxies: double-hump rotation curve or characteristic velocity dispersion profile. It is for this reason that we argue that NGC 5838 is most probably a barred galaxy seen close to end-on (i.e. with the bar parallel to the line-of-sight).

The second peculiar case in our sample is NGC 6010, which is interesting for various reasons. While the level of positive correlation in the fairly round bulge region is low, it is the only case where this correlation becomes very high beyond the bulge. In order to interpret the unusual behaviour of this galaxy, we refer to another interesting part of the study by Iannuzzi & Athanassoula (2015) which discusses the masking effects of a classical bulge on the BP kinematic features. They found that the characteristic sig-

natures of the bar are considerably weakened in the presence of a classical, spherically-symmetric component.

We suggest that NGC 6010 is a barred galaxy with an spherically-symmetric central component, in which the vertical extent of the bar is beyond that of the classical bulge in the center. It may also address the issue that our method to define the bulge analysis window for this galaxy is biased against the presence of a classical bulge in the center. In the other words, the real vertical extent of the bar is further than we already evaluated.

#### 4 QUANTIFYING CYLINDRICAL ROTATION

Kormendy & Illingworth (1982) were the first who reported in the boxy bulge of NGC 4565 line-of-sight velocities that remained almost constant with increasing height above the disk plane. They called this unusual kinematic feature *cylindrical rotation*. This feature was later also reported in several studies (e.g. Bureau & Freeman 1999; Falcón-Barroso et al. 2003a, 2004, 2006), which all confirmed its relation to BP bulges. The good agreement between numerical models and observed kinematics of barred galaxies suggests that cylindrical rotation can be considered as a characteristic behaviour of such systems.

Williams et al. (2011) used long slit spectroscopy to determine that the degree of cylindrical rotation varies significantly among BP bulges. This study argued that BP bulges do not form a homogeneous class of objects. This conclusion, however, was based on a small sample of galaxies. Most of the observed deviations from perfect cylindrical rotation were associated to velocity profiles in slits relatively close to the disk plane, where fast rotating components, thick disks or dust could significantly affect the observed kinematics. It is important to note that the wide range of cylindrical rotation levels in their sample was established qualitatively by visual inspection.

Saha & Gerhard (2013) were the first to introduce a quantitative criterion to measure deviations from pure cylindrical rotation in edge-on disk galaxies. They computed the mean mass weighted line-of-sight velocity of stars, within a set of pseudo-slits along the major axis of model galaxies within the bulge dominated region. They then plotted these values against the slit locations above the

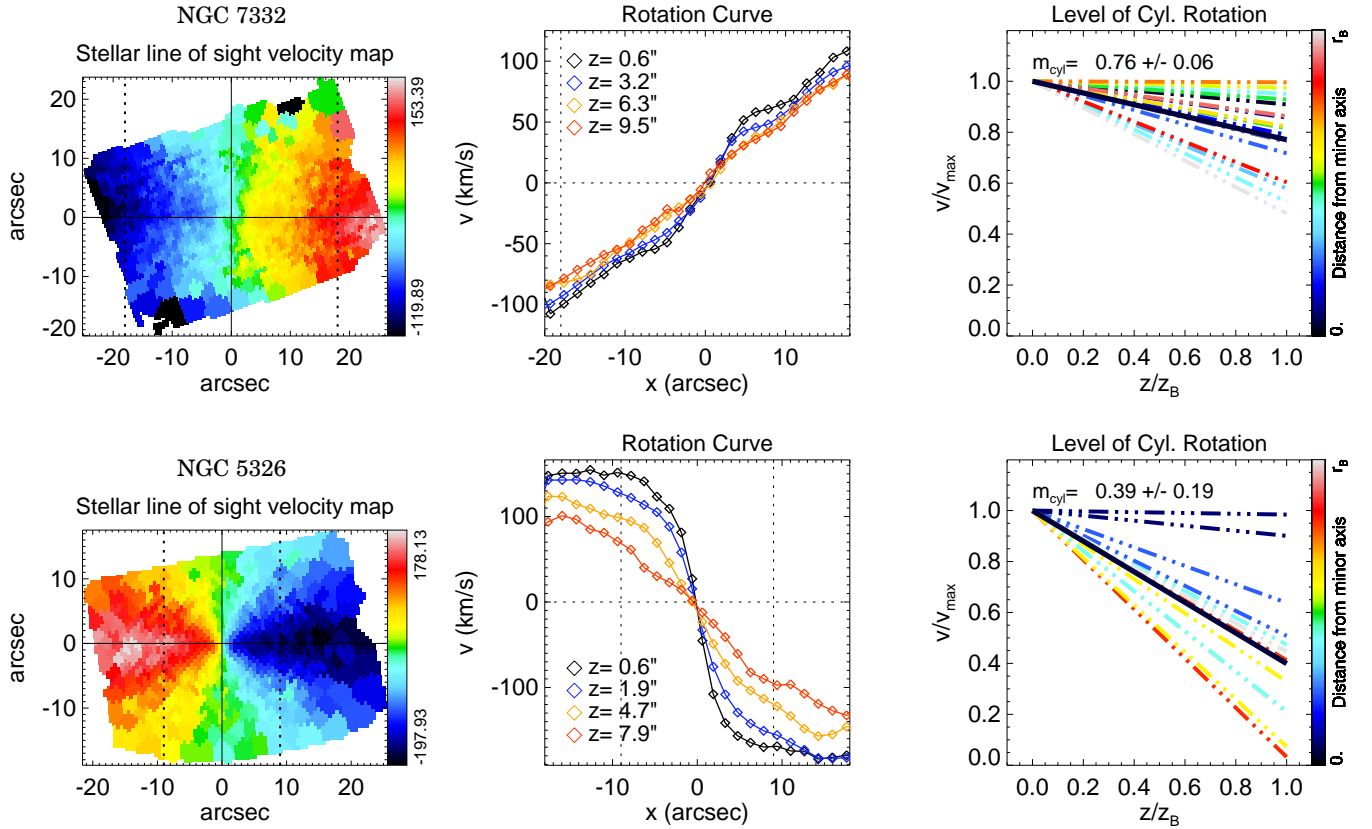


**Figure 4.** (Left) The velocity map of NGC 7332 (a cylindrical rotating system) and NGC 5326 (a non cylindrical rotator). In these plots, velocity maps are rotated so that the horizontal axis is parallel to the major axis of the galaxies. Vertical dotted lines mark the bulge boundaries. (Middle) The stellar line of sight velocity parallel to the major axis of galaxies at different height ( $z$ ) from the disk plane. (Right) Line-of-sight velocity gradient along the minor axis of galaxies at different distance from the minor axis. Profiles are color-coded according to the distance from the minor axis. Solid black profile represents the average value. We define  $m_{\text{cyl}} = m_{\text{avg}} + 1$  as a quantity to express the level of cylindrical rotation, in which  $m_{\text{avg}}$  is the slope of the solid black line. See text for the definition of the various quantities  $m_{\text{cyl}}$ ,  $z_B$  and  $V_{\text{max}}$ .

galactic mid-plane and linearised this profile. They argued that the slope of this linearised profile can be considered as a quantity to express the level of cylindrical rotation. We tested this method with our integral-field data and realised that points farther away from the minor axis have more weight in the calculations and, consequently, the level of cylindrical rotation becomes very sensitive to the definition of bulge boundaries. Moreover, the adopted normalization factor in this method is obtained from the line-of-sight velocity of regions close to disk plane, where the velocity maps of galaxies are strongly affected by complicated nature of contributing components. These issues probably arise by the fact that this method is constructed based on a simplified picture of BP bulges in their  $N$ -body models.

Inspired by the method by Saha & Gerhard (2013), we present here a more robust approach to quantify the level of cylindrical rotation. It is optimised to work with integral-field data. For this purpose, on the clean (i.e., dust-free) side of our galaxies, we define a set of pseudo-slits, parallel to the minor axis of the galaxies at different positions along the major axis, covering the whole horizontal extent of the bulge from  $-x_B$  to  $+x_B$ . The outer slits (with respect to the minor axis) are considered to be wider to compensate for the small number of contributed data points (Voronoi-bins), so that the number of voronoi-bins within all slits is almost the same.

For each pseudo-slit, we plot the absolute value of velocities

against the absolute value of height from the disk plane ( $z$ ). We then fit a straight line to this velocity profile excluding the regions close to disk plane, which are most likely disrupted by contamination of dust and/or central components (evaluated by visual inspection of the velocity maps. This region is marked in Figure 3).

Using this new linear profile, for each pseudo-slit, we evaluate the velocity at  $z=0$  (i.e. the disk of the galaxy). Therefore, we have a set of linearised velocity profiles from  $z=0$  to  $z=z_{\text{bulge}}$  at different distances from the minor axis from  $-x_B$  to  $+x_B$ . Each profile is normalized to its maximum velocity (i.e. for a given slit placed at  $x = x_i$  the profile is normalized to  $V_{\text{max}}^i \equiv V^i(z=0)$ , in which  $V$  is the linearized velocity) and maximum extent of bulge in the  $z$  direction ( $z_B$ ). With this normalization, the slope of this linear profile ranges from -1 to 0. Finally, we calculate the average slope of the linearised velocity profiles related to different slits ( $m_{\text{avg}}$ ) and define  $m_{\text{cyl}} = m_{\text{avg}} + 1$  as a quantity to express the level of cylindrical rotation. With this definition, values of  $m_{\text{cyl}}$  are generally between 1 which presents pure cylindrical rotation and 0 where there is no sign of cylindrical rotation.

Figure 4 illustrates this procedure for two galaxies in our sample: NGC 7332, which is a known barred galaxy with a BP bulge and NGC 5707, a galaxy with an spherical bulge. The figures clearly shows that for NGC 7332 stellar rotation changes very little away from the galaxy mid-plane, while changes in NGC 5707 are much



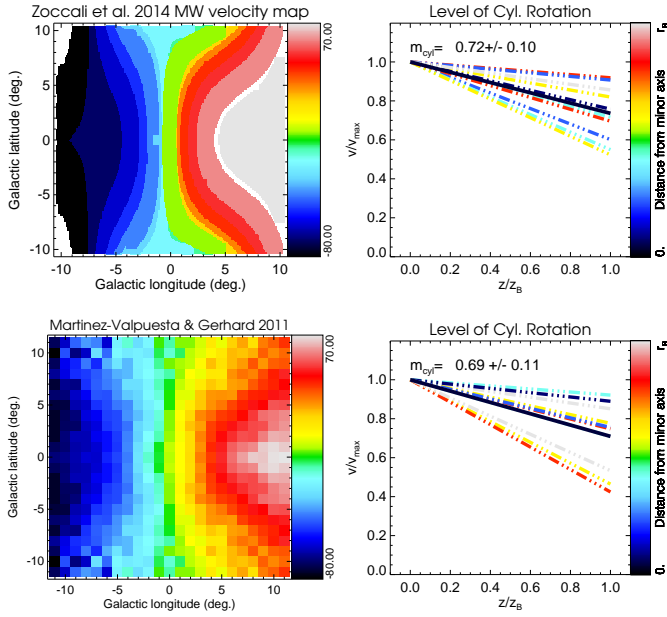


**Figure 5.** (*Top row*) Left panel presents the mean radial velocity map of the Milky Way bulge in the longitude-latitude plane constructed from the measured rotation profiles of Zoccali et al. (2014). The right panel shows the linearised velocity gradient along the minor axis of Milky Way at different distances from the minor axis. Description of the plot is the same as Figure 4 (Right Panel). As discussed in the text, we use these profiles to evaluate the level of cylindrical rotation ( $m_{\text{cyl}}$ ). (*Bottom row*) In the left panel we show a self-consistent  $N$ -body simulation of the Milky Way bulge from Martinez-Valpuesta & Gerhard (2011); Gerhard & Martinez-Valpuesta (2012); Martinez-Valpuesta & Gerhard (2013). The right panel is equivalent to the top, right but for this simulation. Interestingly,  $m_{\text{cyl}}$  for this simulation matches fairly well that coming from real observations.

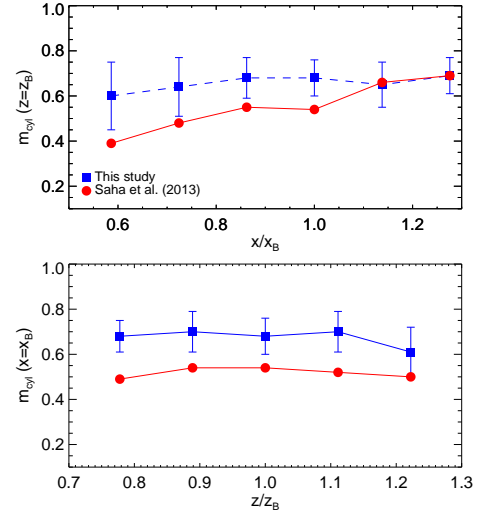
more pronounced. This is also reflected in the spread of the linearised vertical profiles shown in red and blue. Similar figures for the entire sample are presented in Appendix A. We list the measured values of  $m_{\text{cyl}}$  in Table 2.

Figure 6 demonstrates a comparison between the method introduced by Saha & Gerhard (2013) and our new approach to evaluate the level of cylindrical rotation in NGC 0678, a barred galaxy with BP bulge. In the top panel, the bulge radius along the minor axis ( $z$ ) is fixed at  $z_B$  and the level of cylindrical rotation for different values of  $x_B$  has been evaluated using the both methods. In the bottom panel, the  $x_B$  is fixed at a certain value and level of cylindrical rotation is evaluated for different values of  $z_B$ .

While both methods do not show strong dependency to the definition of  $z_B$  (bulge analysis radius along the minor axis), our new approach is more stable against variations along the major axis. This example demonstrates that our method is robust against inner disk components, as NGC 0678 has, and works better than Saha's, at least in cases with noisy profiles.

## 5 CYLINDRICAL ROTATION IN THE MILKY WAY BULGE

It is now widely accepted that the Milky Way (MW) is an example of a barred galaxy with an BP bulge (e.g. Blitz & Spergel 1991; Stanek et al. 1994; Dwek et al. 1995; Babusiaux & Gilmore



**Figure 6.** Level of cylindrical rotation at different major axis (top panel) and minor axis (bottom panel) radii of NGC 0678. In upper panel, the bulge radius along the minor axis ( $z$ ) is fixed to  $z_B$  and the level of cylindrical rotation for different values of  $x_B$  has been evaluated using both Saha & Gerhard (2013) method and the approach, presented in this study. In lower panel, the  $x$  is fixed at a certain value ( $x_B$ ) and level of cylindrical rotation is evaluated for different values of  $z_B$ . As this figure shows, the level of cyl rotation based on our proposed approach shows less sensitivity to the definition of  $x_B$  compare to the Saha & Gerhard (2013) method. The dependency of both methods to the bulge analysis radius along the minor axis ( $x_B$ ) is negligible.

2005; Rattenbury et al. 2007). As we are situated in the disk plane, the detailed analysis of Galactic bulge kinematics is a non-trivial task. During the past decade, different surveys of the Galactic bulge have described a clearer picture of the Galactic bulge. Cylindrical rotation was first established in the MW bulge from data at latitudes between  $b = -2$  and  $b = -8$  by the BRAVA survey (Rich et al. 2007; Howard et al. 2009; Kunder et al. 2012). More recently, the Giraffe Inner Bulge Survey (Zoccali et al. 2014), carried out at the ESO-VLT with the multi-fibre spectrograph FLAMES, targeted around 5000 red clump giants. The primary goal of this survey is to characterize the kinematics, metallicity distribution, and element ratio of those stars across 31 fields in the Galactic bulge region. These results confirmed previous claims of cylindrical rotation. Zoccali et al. (2014) also presented radial velocity, and velocity dispersion maps of the MW bulge, by interpolating the measured values of radial velocity and velocity dispersion at different observed locations at negative latitudes. They also used data at  $b = 4.5$  in order to verify the assumption of symmetry with respect to galactic plane. In the context of our work in this paper, these maps are very useful as they allow for direct comparison of the Galactic bulge kinematic maps with those of external galaxies.

We have taken advantage of this opportunity and applied our method to quantify the level of cylindrical rotation in the MW bulge. Figure 5 (top row) shows the velocity map extracted from the Zoccali et al. (2014) article. Based on our measurements, the degree of cylindrical rotation ( $m_{\text{cyl}}$ ), within the whole available area ( $-10 < l < +10$  and  $-10 < b < +10$ ), evaluated by Zoccali et al. (2014) is  $0.72 \pm 0.1$ .

In addition, we have also applied this method to the same scaled area from the  $N$ -body simulation of Martinez-Valpuesta & Gerhard (2011, hereafter MVG11),



which was known to match remarkably well the structure of the MW bulge (Gerhard & Martinez-Valpuesta 2012; Martinez-Valpuesta & Gerhard 2013). In the MVG11 model of the MW, the bar length is  $\sim 4.5 kpc$ , oriented at an angle  $\alpha = 25^\circ$  with respect to the line from the Galactic center to the observer. Perhaps not surprisingly, the  $m_{cyl}$  value for this simulation is very much consistent with what we measured from the Zoccali et al. (2014) observations. However, as the color profiles in right panels of figure 5 show, the velocity pattern for these two cases is not alike<sup>2</sup>, while the representative (mean) values, for both cases, show a high level of cylindrical rotation. These results show that the MW bulge is cylindrically rotating at the same level as the strongest objects in our sample of external galaxies.

To address any concern regarding the field size mismatch between the MW and our sample galaxies, for estimating  $m_{cyl}$ , we refer to Figure 7, in which we also present the variation of  $m_{cyl}$  with inclination and PA based on the simulated galaxies of MVG11 for which the disk subtraction has been carried out as in the sample galaxies. The variation in the region of interest (*Inclination*  $i = 90^\circ$  and *Bar PA*  $= 65^\circ$ ), which matches that of the MW, is smooth and the  $m_{cyl}$  value is quite similar ( $\sim 0.7$ ) to the value obtained from Zoccali et al. (2014).

## 6 DISCUSSION

In this section we summarise our results regarding the presence of bars and level of cylindrical rotation for the entire sample, and discuss the limitations of the diagnostics described above. In Table 2, we list our findings in terms of kinematic features, boxiness, and cylindrical rotation of the bulges in our sample.

### 6.1 Kinematic signatures of bars in our sample

We analysed the two dimensional kinematics maps of a sample of 12 intermediate inclined ( $i > 60^\circ$ ) galaxies. As established with our image decomposition and unsharp masked images (see Figure 2), 50% of galaxies in this sample contain BP bulges (NGC 0678, NGC 5422, NGC 5689, NGC 5746, NGC 5965, NGC 7332). The linear correlation profiles of all these 6 galaxies reveal strong  $V - h_3$  anti-correlation within the central, few arcsec region. This feature is associated to observed fast rotating, axisymmetric inner disks, most likely formed secularly through bar-driven processes. Due to the axisymmetric nature of such structures, the related kinematic signatures will be largely independent of viewing angle. Another common feature in these 6 galaxies is the positive correlations between the velocity and  $h_3$  beyond the central regions in areas dominated by the BP bulge light. All these galaxies also display double-hump velocity profiles and fairly broad velocity dispersion profiles (see Appendix A). In addition they present the highest levels of cylindrical rotation. All this information combined confirm that the observed BP bulges are strongly linked to bar structures.

At the opposite end, there are 4 galaxies (NGC 5326, NGC 5475, NGC 5707, NGC 6010) with nearly spherical bulges and no indication of bars being present based on their kinematic

information. None of these galaxies are known in the literature to host bars. The level of cylindrical rotation in these bulges are also the lowest of the sample and thus confirms the kinematic diagnostics. NGC 6010 is a special case among these four galaxies. The level of positive  $V - h_3$  correlation above the bulge dominated region is quite large, it also shows a strong anti-correlation in the inner parts (possibly indicating the presence of an inner disk). There is, however, no sign of strong double-hump velocity profiles or broad velocity dispersion major axis profiles.

As discussed in §3, we suggest that NGC 6010 is a barred galaxies with an spherically-symmetric central component, in which the vertical extend of the bar is beyond the classical bulge in the center. With this configuration we can interpret the unusual kinematical behavior of this galaxy which is very similar to unbarred systems within the bulge zone and similar to barred galaxies beyond that.

As already pointed out in §3, another interesting case is NGC 5838. It has a fairly round bulge but presents kinematic features remarkably similar to those of strongly barred galaxies listed above. It shows a strong anti-correlation in the inner parts and positive correlation away from the disk plane, in the bulge dominated regions. The major axis kinematic profiles also show clear double-hump rotation and broad central velocity dispersion. The only feature that differs from those exhibited by strong barred systems is the low level of cylindrical rotation measured. As we explain in the next section, this is expected if the bar is oriented parallel to our line-of-sight. Therefore we propose that this galaxy is in fact barred.

There is only one exception in our sample (NGC 7457) in which the level of cylindrical rotation is considerably high ( $m_{cyl} > 0.7$ ), but the photometric and kinematics properties of this galaxy suggest there is no bar present. Sil'chenko et al. (2002) analysed the two-dimensional kinematics maps of this peculiar galaxy in detail and proposed that this galaxy is the result of two superposed quasi-counter-rotating stellar disks with different inclinations. At this point, it is not obvious whether the high level of cylindrical rotation measured could be linked to this peculiar orbital configuration or not, although some studies suggest that axisymmetric configurations can in certain circumstances also give rise to cylindrical rotation (e.g. Rowley 1988). NGC 7457 is therefore a very peculiar case in our study.

Our results suggest that 8 out of 12 galaxies in our sample contain bars, with at least one of them (NGC 5838), possibly 2 (NGC 6010), being new identifications. Based on the results presented here we confirm that the major-axis stellar kinematic diagnostics presented by Bureau & Athanassoula (2005) and the extension of this method to the 2D line-of-sight kinematics of simulated disk galaxies by Iannuzzi & Athanassoula (2015) are reliable discriminators for determination of the presence of bars in highly inclined systems. We show that the  $V - h_3$  correlation profiles are particularly useful for this purpose. Cylindrical rotation is another important feature of barred systems, but it is not always a good discriminant as it depends on the galaxy's inclination and bar orientation along the line-of-sight. In the following section we characterise these changes in cylindrical rotation using  $N$ -body simulations.

### 6.2 The effect of bar orientation and galaxy inclination on the level of cylindrical rotation

Our observational results confirm a close link between the morphology and kinematics of barred disk galaxies. We also show that cylindrical rotation appears to be sensitive to the particular configuration between the galaxy inclination and the bar posi-

<sup>2</sup> Note that, the velocity map, presented by Zoccali et al. (2014) is an inferred map from discrete data points, not homogeneously covering the  $l-b$  grid, while in the MVG11 model of MW bulge (Bottom row of Figure 5), all the particles in the line of sight have been included. This could explain the discrepancies between these two velocity fields.

**Table 2.** Bar signatures and Bulge classification.

NGC number	0678	5326	5422	5475	5689	5707	5746	5838	5965	6010	7332	7457
1) Double-hump rotation curve	Y	N	Y	N	Y	N	Y	Y	Y	N?	Y	N
2) Broad central $\sigma$ peak with plateau at moderate radii	N?	N	N?	N	Y	N	Y	Y	Y	N	Y	N
3) $V - h_3$ correlation over the projected bar length	Y	N	Y	N	Y	N	Y	Y	Y	N	Y	N
Central $V - h_3$ anti-correlation	Y	N	Y	Y	Y	N	Y	Y	Y	Y	Y	N
Boxy/Peanut Bulge	Y	N	Y	N	Y	N	Y	N	Y	N	Y	N
<b>Degree of Cyl. Rotation (<math>m_{\text{cyl}}</math>)</b>	0.66 $\pm 0.09$	0.39 $\pm 0.19$	0.70 $\pm 0.07$	0.44 $\pm 0.17$	0.64 $\pm 0.09$	0.22 $\pm 0.21$	0.63 $\pm 0.08$	0.40 $\pm 0.17$	0.62 $\pm 0.10$	0.42 $\pm 0.17$	0.76 $\pm 0.06$	0.78 $\pm 0.08$
<b>Bar</b>	Y	N	Y	N	Y	N	Y	Y	Y	Y?	Y	N

NOTES: In this table, the "Y" refers to Yes and "N" refers to No answer. The Question mark (?) next to few answers demonstrates the uncertainty in those answers. The upper section of the table shows the characteristic of the  $V$ ,  $\sigma$  and  $h_3$  profiles, which are extracted only on the clean (i.e. dust-free) side of our galaxies, along the major axis at different height from the disk plane. The (anti)correlation between the  $V$  and  $h_3$  are studied in details in §3 and the results are presented in §3. The second panel of this table presents our classification of the bulge-type by visually inspecting the unsharp-masked images as well as the residual images after subtracting an exponential disk model from the original images (we refer the reader to §2.1 for more details). The last panels present the degree or cylindrical rotation ( $m_{\text{cyl}}$ ) for our galaxies, as described in §4. Based on the bar diagnostics, presented, we label our galaxies as barred or non-barred in the last row.

tion angle with respect to our line-of-sight. To illustrate this dependency we use kinematic maps extracted from self-consistent three-dimensional  $N$ -body simulations of a boxy bulge and bar which formed from a bar-unstable disk by Martínez-Valpuesta et al. (2006, hereafter IMV06) and Martínez-Valpuesta & Gerhard (2011, hereafter MVG11). We treat these maps in the same way we deal with the observed data, considering the method to evaluate the bulge analysis window, thus computed the  $m_{\text{cyl}}$  values in a consistent manner. The I1 series of the MVG11 that we have used here, evolved from an initially exponential disk with  $Q = 1.5$  embedded in a dark matter halo, and developed a prominent boxy bulge through a buckling instability after  $\sim 1.5$  Gyr. Figure 7 presents the result of this exercise for a particular snapshot in this simulation, when the bar and its BP bulge has fully developed. The figure shows how the level of cylindrical rotation changes as a function of galaxy inclination and bar position angle. As shown in Martínez-Valpuesta & Athanassoula (2008), the strength of the bar correlates with the strength of the BP bulge, and therefore the absolute values displayed in the figure depend somewhat on the strength of the bar. Nevertheless, the general behavior is the same for all cases studied. The figure shows that when the bar is oriented perpendicular to our line-of-sight, cylindrical rotation hardly changes with galaxy inclination (for values above  $60^\circ$  at least). This suggests that, while the presence of the main disk of the galaxy is becoming more and more important along our line-of-sight as we depart from edge-on inclination, its effect is not significant when it comes to affect the  $m_{\text{cyl}}$  measurements. At edge-on inclination, it seems that the orientation of the bar is not an obstacle to measure high levels of cylindrical rotation in barred systems. Nevertheless, the situation changes as inclination decreases and the bar is oriented parallel to our line-of-sight. We believe this effect may be at the root of the low levels of cylindrical rotation observed in NGC 5838, while the other kinematic diagnostics clearly suggest the presence of a bar in the galaxy.

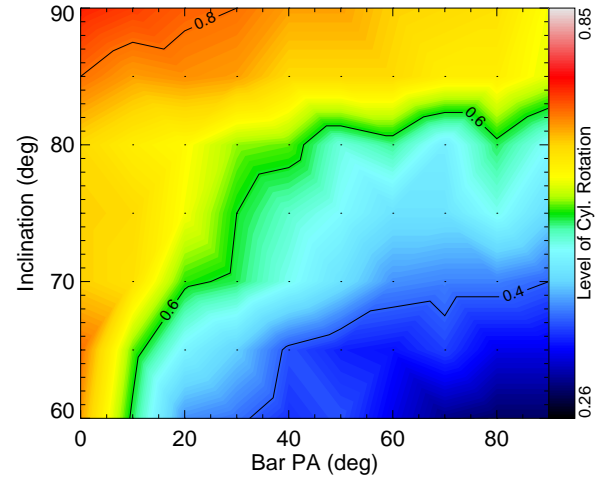


**Figure 7.** Level of cylindrical rotation ( $m_{\text{cyl}}$ ) in a  $N$ -body simulation of a bar-unstable disk for different galaxy inclinations and bar position angle. The range of galaxy inclinations explored here is similar to the ones of our sample of galaxies. In this figure, a side-on bar (i.e. perpendicular to the line-of-sight) has a Bar PA of  $0^\circ$ , while an end-on bar (i.e. parallel to the line-of-sight) has  $90^\circ$ . Small dots mark the reference locations of  $m_{\text{cyl}}$  values in our simulations. The colour map shows intermediate levels, interpolated from the reference points.

### 6.3 Cylindrical rotation in bulges of nearby galaxies

In previous sections we have established a new methodology to compute the level of cylindrical rotation ( $m_{\text{cyl}}$ ) in galaxies and also described some of the potential shortcomings of this parameter. Here we will concentrate on presenting the distribution of  $m_{\text{cyl}}$  values for our sample of galaxies, and also what one would expect in general based on results from our numerical simulations.

Figure 8 (top panel) shows the distribution of  $m_{\text{cyl}}$  values for our sample. Perhaps not surprisingly, all the galaxies with

BP bulges display levels of cylindrical rotation above  $\approx 0.6$ . As mentioned earlier, the MW bulge  $m_{\text{cyl}}$  value is very consistent with those of BP bulges. Galaxies with no signs to host bars, on the other hand, have  $m_{\text{cyl}}$  values below  $\approx 0.5$ . The only peculiar case of a non-barred galaxy with high  $m_{\text{cyl}}$  values is NGC 7457 (see §6.1 for details). At the low  $m_{\text{cyl}}$  end we also have the two galaxies that we believe harbour bars in an end-on orientation (NGC 5838, NGC 6010).

While our sample is admittedly limited, it serves to see the range of possible values of  $m_{\text{cyl}}$  in galaxies. The location of BP and spherical bulges is clearly distinct, but with the low number statistics is difficult to assess the degree of overlap between these two families of objects.

In order to understand the expected true distribution of this parameter, we have resorted to the set of  $N$ -body simulations (IMV06, MVG11) used in the previous section, complemented with a set of numerical simulations of barred galaxies with classical bulges, evolved from an exponential disk and a classical bulge embedded in a live dark matter halo, with  $B/D = 0.25$  and  $Q = 1.5$ . For these simulations, “non-barred” refers to the stage when the bar is flat and “barred”, after the boxy bulge has formed and the bar has regrown. The results are shown in Figure 8 (bottom panel). We present the results for non-barred galaxies in blue and barred galaxies in red.

For barred systems, we plot values of  $m_{\text{cyl}}$  for a wide range of different time snapshots and combinations of galaxy inclination (above  $60^\circ$ ) and bar position angle. The distributions of the two kind of objects clearly separated with mean values  $0.35 \pm 0.10$  for non barred systems and  $0.65 \pm 0.15$  for barred galaxies. The distribution for barred galaxies, however, shows cases with low  $m_{\text{cyl}}$  values, overlapping regions dominated by galaxies with no bars. These are cases where the bar position angle and galaxy inclination are in unfavourable orientations (see Figure 7). This result is in agreement with previous studies by Athanassoula & Misiriotis (2002) and Iannuzzi & Athanassoula (2015) which indicate the effect of the viewing angles on the measured level of cylindrical rotation in simulated disk galaxies. They indicate a tendency for cylindrical rotation to weaken when going from side-on to end-on views. They also stress that the importance of this effect does not follow a clear trend with BP strength and link such behaviour to the different orbital structure in each bar and on various properties of the periodic orbits of the main families.

Our observations and the complementary numerical tests thus confirm that cylindrical rotation is a reliable indicator for the presence of bars only when its levels are high. Low  $m_{\text{cyl}}$  values are not definite prove of the absence of bars.

## 7 CONCLUSIONS

This paper investigates the connection between bulge morphology and kinematics in 12 mid to high-inclination ( $i > 60^\circ$ ) disk galaxies, from the Balcells & Peletier (1994) sample, observed with the SAURON integral-field spectrograph. The goal was to unveil the presence of hidden bars, using the major axis kinematic diagnostics developed by (Bureau & Athanassoula 2005) and (Iannuzzi & Athanassoula 2015, optimised for 2D kinematic data) and establish the overall level of cylindrical rotation ( $m_{\text{cyl}}$ ) in those bulges. For the latter, we developed a new method (inspired by the work of Saha & Gerhard 2013) that quantifies the importance of this property in our bulges.

We find that the strong positive correlation between the stellar

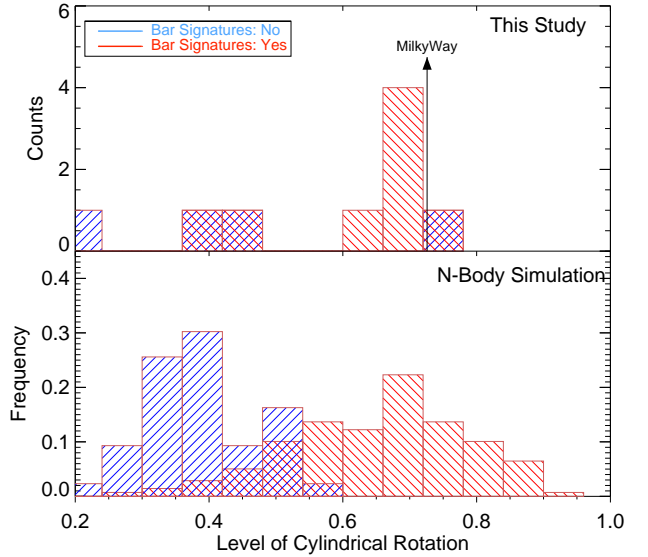


**Figure 8.** Distribution of the level of cylindrical rotation ( $m_{\text{cyl}}$ ) for observations (top panel) and in  $N$ -body simulations (bottom panel). For the observations, galaxies with clear signatures of bars are marked in red, while those with no signs are in blue. In the simulations, non-barred galaxies are marked in blue and barred systems in red.

velocity ( $V$ ) and the  $h_3$  Gauss-Hermite parameter appears to be the most reliable indicator for the presence of bars among all other bar diagnostics. This is true even in situations when the bar orientation is parallel to line-of-sight and consequently the bar not clearly visible in photometric data. We exploited this feature and determined that 8 galaxies in our sample harbour bar structures. While some of them were known or were very obvious cases, we have identified 3 new cases based on their kinematic properties (NGC 5422, NGC 5838, NGC 6010).

Bulges in our sample display a wide range of cylindrical rotation values, with BP bulges showing the largest levels ( $m_{\text{cyl}} \approx 0.7$ ). Using the same methodology, we have established that the Milky Way bulge shows comparable levels of cylindrical rotation ( $m_{\text{cyl}} = 0.72 \pm 0.1$ ) to the BP bulges of external galaxies. Nearly spherical bulges (e.g. non-barred galaxies) display values around  $m_{\text{cyl}} \approx 0.35$ .

Our study with  $N$ -body simulations confirms that high levels of cylindrical rotation can be considered in general as a common feature of strongly barred galaxies (e.g. BP bulges). The opposite is not true though, as particular orientations of the bar along the line-of-sight (e.g. end-on bars) display relatively low values of  $m_{\text{cyl}}$  (levels in fact comparable to unbarred galaxies). Therefore cylindrical rotation cannot be considered a reliable kinematic property to identify the full population of barred galaxies. The same simulations suggest that the distribution of  $m_{\text{cyl}}$  for barred and non-barred galaxies have clearly distinct mean values. Nonetheless, there is significant overlap in the low-end caused by non-favourable galaxy and barred orientations (i.e. galaxy low-inclination, and bar position angle close to  $90^\circ$ ) or flat bar phases.

In summary, focusing on the study of the kinematic properties of intermediate inclined galaxies, we have unveiled the presence of bars and also established the level of cylindrical rotation in bulges in general. In the following paper of this series we will relate these



properties to the stellar content in these bulges, paying particular attention to the impact of cylindrical rotation to the age and metallicity gradients away from the mid-plane of these galaxies.

## ACKNOWLEDGMENTS

The first author wish to thank the School of Astronomy, IPM for providing support while working on this paper. A.M. also acknowledges the Isaac Newton Group of Telescopes (ING) and the Instituto de Astrofísica de Canarias (IAC) for hospitality and support while this paper was in progress. We also thank an anonymous referee for a lot of constructive comments. The authors acknowledge support from the Spanish Ministry of Economy and Competitiveness (MINECO) through grants AYA2009-11137, AYA2013-48226-C3-1-P, AYA2013-46886-P and AYA2014-58308-P. J.F.B. also acknowledges financial support from the DAGAL network from the People Programme (Marie Curie Actions) of the European Unions Seventh Framework Programme FP7/2007-2013/ under REA grant agreement number PITN-GA-2011-289313.

Funding for SDSS-III has been provided by the Alfred P. Sloan Foundation, the Participating Institutions, the National Science Foundation, and the U.S. Department of Energy Office of Science. The SDSS-III web site is <http://www.sdss3.org/>. SDSS-III is managed by the Astrophysical Research Consortium for the Participating Institutions of the SDSS-III Collaboration including the University of Arizona, the Brazilian Participation Group, Brookhaven National Laboratory, Carnegie Mellon University, University of Florida, the French Participation Group, the German Participation Group, Harvard University, the Instituto de Astrofísica de Canarias, the Michigan State/Notre Dame/JINA Participation Group, Johns Hopkins University, Lawrence Berkeley National Laboratory, Max Planck Institute for Astrophysics, Max Planck Institute for Extraterrestrial Physics, New Mexico State University, New York University, Ohio State University, Pennsylvania State University, University of Portsmouth, Princeton University, the Spanish Participation Group, University of Tokyo, University of Utah, Vanderbilt University, University of Virginia, University of Washington, and Yale University.

## REFERENCES

- Ahn C. P., Alexandroff R., Allende Prieto C., Anders F., Anderson S. F., Anderton T., Andrews B. H., Aubourg É., Bailey S., Bastien F. A., et al. 2014, *ApJS*, 211, 17
- Athanassoula E., 2015, *ArXiv e-prints*
- Athanassoula E., Beaton R. L., 2006, *MNRAS*, 370, 1499
- Athanassoula E., Misiriotis A., 2002, *MNRAS*, 330, 35
- Babusiaux C., Gilmore G., 2005, *MNRAS*, 358, 1309
- Bacon R., Copin Y., Monnet G., Miller B. W., Allington-Smith J. R., Bureau M., Carollo C. M., Davies R. L., Emsellem E., Kuntschner H., Peletier R. F., Verolme E. K., de Zeeuw P. T., 2001, *MNRAS*, 326, 23
- Balcells M., Graham A. W., Domínguez-Palmero L., Peletier R. F., 2003a, *ApJ*, 582, L79
- Balcells M., Graham A. W., Domínguez-Palmero L., Peletier R. F., 2003b, *ApJ*, 582, L79
- Balcells M., Graham A. W., Peletier R. F., 2007a, *ApJ*, 665, 1084
- Balcells M., Graham A. W., Peletier R. F., 2007b, *ApJ*, 665, 1104
- Balcells M., Peletier R. F., 1994, *AJ*, 107, 135
- Berentzen I., Heller C. H., Shlosman I., Fricke K. J., 1998, *MNRAS*, 300, 49
- Berentzen I., Shlosman I., Martinez-Valpuesta I., Heller C. H., 2007, *ApJ*, 666, 189
- Bettoni D., Galletta G., 1997, *A&AS*, 124, 61
- Blitz L., Spergel D. N., 1991, *ApJ*, 379, 631
- Bundy K., Bershadsky M. A., Law D. R., Yan R., Drory N., MacDonald N., Wake D. A., Cherinka B., et al. 2015, *ApJ*, 798, 7
- Bureau M., Athanassoula E., 2005, *ApJ*, 626, 159
- Bureau M., Athanassoula E., Chung A., Aronica G., 2004, in Block D. L., Puerari I., Freeman K. C., Groess R., Block E. K., eds, *Penetrating Bars Through Masks of Cosmic Dust Vol. 319 of Astrophysics and Space Science Library*, Bar-Driven Evolution and 2D Spectroscopy of Bulges. p. 139
- Bureau M., Freeman K. C., 1999, *AJ*, 118, 126
- Buta R. J., Sheth K., Athanassoula E., Bosma A., Knapen J. H., Laurikainen E., Salo H., 2015, *ApJS*, 217, 32
- Cappellari M., Copin Y., 2003, *MNRAS*, 342, 345
- Cappellari M., Emsellem E., 2004, *PASP*, 116, 138
- Cappellari M., Emsellem E., Krajnović D., McDermid R. M., Scott N., Verdoes Kleijn G. A., et al. 2011, *MNRAS*, 413, 813
- Cappellari M., Emsellem E., Krajnović D., McDermid R. M., Scott N., Verdoes Kleijn G. A., Young L. M., Alatalo K., et al. 2011, *MNRAS*, 413, 813
- Cappellari M., McDermid R. M., Alatalo K., Blitz L., Bois M., Bournaud F., 2013, *MNRAS*, 432, 1862
- Chung A., Bureau M., 2004, *AJ*, 127, 3192
- Combes F., Debbasch F., Friedli D., Pfenniger D., 1990, *A&A*, 233, 82
- Combes F., Sanders R. H., 1981, *A&A*, 96, 164
- Croom S. M., Lawrence J. S., Bland-Hawthorn J., Bryant J. J., Fogarty L., Richards S., Goodwin M., Farrell T., et al. 2012, *MNRAS*, 421, 872
- de Vaucouleurs G., de Vaucouleurs A., Corwin Jr. H. G., Buta R. J., Paturel G., Fouqué P., 1991, *Third Reference Catalogue of Bright Galaxies. Volume I: Explanations and references. Volume II: Data for galaxies between 0<sup>h</sup> and 12<sup>h</sup>. Volume III: Data for galaxies between 12<sup>h</sup> and 24<sup>h</sup>.*
- Debattista V. P., Mayer L., Carollo C. M., Moore B., Wadsley J., Quinn T., 2006, *ApJ*, 645, 209
- Dwek E., Arendt R. G., Hauser M. G., Kelsall T., Lisse C. M., Moseley S. H., Silverberg R. F., Soderoski T. J., Weiland J. L., 1995, *ApJ*, 445, 716
- Emsellem E., Greusard D., Combes F., Friedli D., Leon S., Pécontal E., Wozniak H., 2001, *A&A*, 368, 52
- Erwin P., Debattista V. P., 2013, *MNRAS*, 431, 3060
- Eskridge P. B., Frogel J. A., Pogge R. W., Quillen A. C., Davies R. L., DePoy D. L., Houdashelt M. L., Kuchinski L. E., Ramírez S. V., Sellgren K., Terndrup D. M., Tiede G. P., 2000, *AJ*, 119, 536
- Falcón-Barroso J., Bacon R., Bureau M., Cappellari M., Davies R. L., de Zeeuw P. T., Emsellem E., Fathi K., Krajnović D., Kuntschner H., McDermid R. M., Peletier R. F., Sarzi M., 2006, *MNRAS*, 369, 529
- Falcón-Barroso J., Balcells M., Peletier R. F., Vazdekis A., 2003, *A&A*, 405, 455
- Falcón-Barroso J., Peletier R. F., Balcells M., 2002, *MNRAS*, 335, 741
- Falcón-Barroso J., Peletier R. F., Emsellem E., Kuntschner H., Fathi K., Bureau M., Bacon R., Cappellari M., Copin Y., Davies R. L., de Zeeuw T., 2004, *MNRAS*, 350, 35
- Falcón-Barroso J., Peletier R. F., Vazdekis A., Balcells M., 2003,

- ApJ, 588, L17
- Falcón-Barroso J., Sánchez-Blázquez P., Vazdekis A., Ricciardelli E., Cardiel N., Cenarro A. J., Gorgas J., Peletier R. F., 2011, A&A, 532, A95
- Friedli D., Benz W., 1993, A&A, 268, 65
- Gadotti D. A., 2008, MNRAS, 384, 420
- Ganda K., Falcón-Barroso J., Peletier R. F., Cappellari M., Emsellem E., McDermid R. M., de Zeeuw P. T., Carollo C. M., 2006, MNRAS, 367, 46
- Gerhard O., Martinez-Valpuesta I., 2012, ApJ, 744, L8
- Ghosh B. K., 1966, Biometrika, 53, pp. 258
- Grosbøl P., Patsis P. A., Pompei E., 2004, A&A, 423, 849
- Howard C. D., Rich R. M., Clarkson W., Mallery R., Kormendy J., De Propris R., Robin A. C., Fux R., Reitzel D. B., Zhao H. S., Kuijken K., Koch A., 2009, ApJ, 702, L153
- Iannuzzi F., Athanassoula E., 2015, MNRAS, 450, 2514
- Kent S. M., 1984, ApJS, 56, 105
- Knapen J. H., Shlosman I., Peletier R. F., 2000, ApJ, 529, 93
- Kormendy J., 1983, ApJ, 275, 529
- Kormendy J., Illingworth G., 1982, ApJ, 256, 460
- Kuijken K., Merrifield M. R., 1995, ApJ, 443, L13
- Kunder A., Koch A., Rich R. M., de Propris R., Howard C. D., Stubbs S. A., Johnson C. I., Shen J., Wang Y., Robin A. C., Kormendy J., Soto M., Frinchaboy P., Reitzel D. B., Zhao H., Origlia L., 2012, AJ, 143, 57
- Lütticke R., 1996, PhD thesis, Diploma Thesis, Ruhr-Universität Bochum, (1996)
- Lütticke R., Dettmar R.-J., Pohlen M., 2000, A&AS, 145, 405
- Marinova I., Jogee S., 2007, ApJ, 659, 1176
- Márquez I., Masegosa J., Durret F., González Delgado R. M., Moles M., Maza J., Pérez E., Roth M., 2003, A&A, 409, 459
- Martínez-Valpuesta I., Athanassoula E., 2008, in Knapen J. H., Mahoney T. J., Vazdekis A., eds, Pathways Through an Eclectic Universe Vol. 390 of Astronomical Society of the Pacific Conference Series, Boxy/Peanut Bulges and Stellar Bars. p. 463
- Martinez-Valpuesta I., Gerhard O., 2011, ApJ, 734, L20
- Martinez-Valpuesta I., Gerhard O., 2013, ApJ, 766, L3
- Martinez-Valpuesta I., Shlosman I., 2004, ApJ, 613, L29
- Martinez-Valpuesta I., Shlosman I., Heller C., 2006, ApJ, 637, 214
- Merrifield M. R., Kuijken K., 1999, A&A, 345, L47
- Peletier R. F., Balcells M., 1996, AJ, 111, 2238
- Peletier R. F., Balcells M., 1997, New A, 1, 349
- Peletier R. F., Balcells M., Davies R. L., Andredakis Y., Vazdekis A., Burkert A., Prada F., 1999, MNRAS, 310, 703
- Pence W. D., 1981, ApJ, 247, 473
- Peng C. Y., Ho L. C., Impey C. D., Rix H.-W., 2002, AJ, 124, 266
- Pérez I., Sánchez-Blázquez P., Zurita A., 2009, A&A, 495, 775
- Raha N., Sellwood J. A., James R. A., Kahn F. D., 1991, Nature, 352, 411
- Rattenbury N. J., Mao S., Sumi T., Smith M. C., 2007, MNRAS, 378, 1064
- Rich R. M., Reitzel D. B., Howard C. D., Zhao H., 2007, ApJ, 658, L29
- Rowley G., 1988, ApJ, 331, 124
- Saha K., Gerhard O., 2013, MNRAS, 430, 2039
- Saha K., Martinez-Valpuesta I., Gerhard O., 2012, MNRAS, 421, 333
- Saha K., Pfenniger D., Taam R. E., 2013, ApJ, 764, 123
- Sánchez S. F., Kennicutt R. C., Gil de Paz A., van de Ven G., Vílchez J. M., Wisotzki L., Walcher C. J., Mast D., et al. 2012, A&A, 538, A8
- Sellwood J. A., Wilkinson A., 1993, Reports on Progress in Physics, 56, 173
- Shaw M. A., Combes F., Axon D. J., Wright G. S., 1993, A&A, 273, 31
- Sil'chenko O. K., Afanasiev V. L., Chavushyan V. H., Valdes J. R., 2002, ApJ, 577, 668
- Stanek K. Z., Mateo M., Udalski A., Szymanski M., Kaluzny J., Kubiak M., 1994, ApJ, 429, L73
- Taylor J. R., 1996, An Introduction to Error Analysis: The Study of Uncertainties in Physical Measurements, 2 sub edn. University Science Books
- Vazdekis A., Sánchez-Blázquez P., Falcón-Barroso J., Cenarro A. J., Beasley M. A., Cardiel N., Gorgas J., Peletier R. F., 2010, MNRAS, 404, 1639
- Villa-Vargas J., Shlosman I., Heller C., 2010, ApJ, 719, 1470
- Whyte L. F., Abraham R. G., Merrifield M. R., Eskridge P. B., Frogel J. A., Pogge R. W., 2002, MNRAS, 336, 1281
- Williams M. J., Zamojski M. A., Bureau M., Kuntschner H., Merrifield M. R., de Zeeuw P. T., Kuijken K., 2011, MNRAS, 414, 2163
- Wozniak H., Combes F., Emsellem E., Friedli D., 2003, A&A, 409, 469
- Wozniak H., Michel-Dansac L., 2009, A&A, 494, 11
- Zoccali M., Gonzalez O. A., Vasquez S., Hill V., Rejkuba M., Valenti E., Renzini A., Rojas-Arriagada A., Martinez-Valpuesta I., Babusiaux C., Brown T., Minniti D., McWilliam A., 2014, A&A, 562, A66

## APPENDIX A: KINEMATIC MAPS FOR INDIVIDUAL GALAXIES

For each galaxy we present here the integrated flux, stellar velocity,  $\sigma$ ,  $h_3$  and  $h_4$  maps. The bulge radius along the major axis is marked with black dash lines. We also present radial profiles for the velocity,  $\sigma$ ,  $h_3$  and  $h_4$  along the major axis of galaxies at 4 different heights from the mid-plane. These heights ( $z$ ) are selected so that, one profile is close to disk plane and one is close to the bulge border in  $z$  direction and two profiles in between. We also show the degree of cylindrical rotation  $m_{\text{cyl}}$  for each galaxy.

## NGC 0678

## NGC 5326

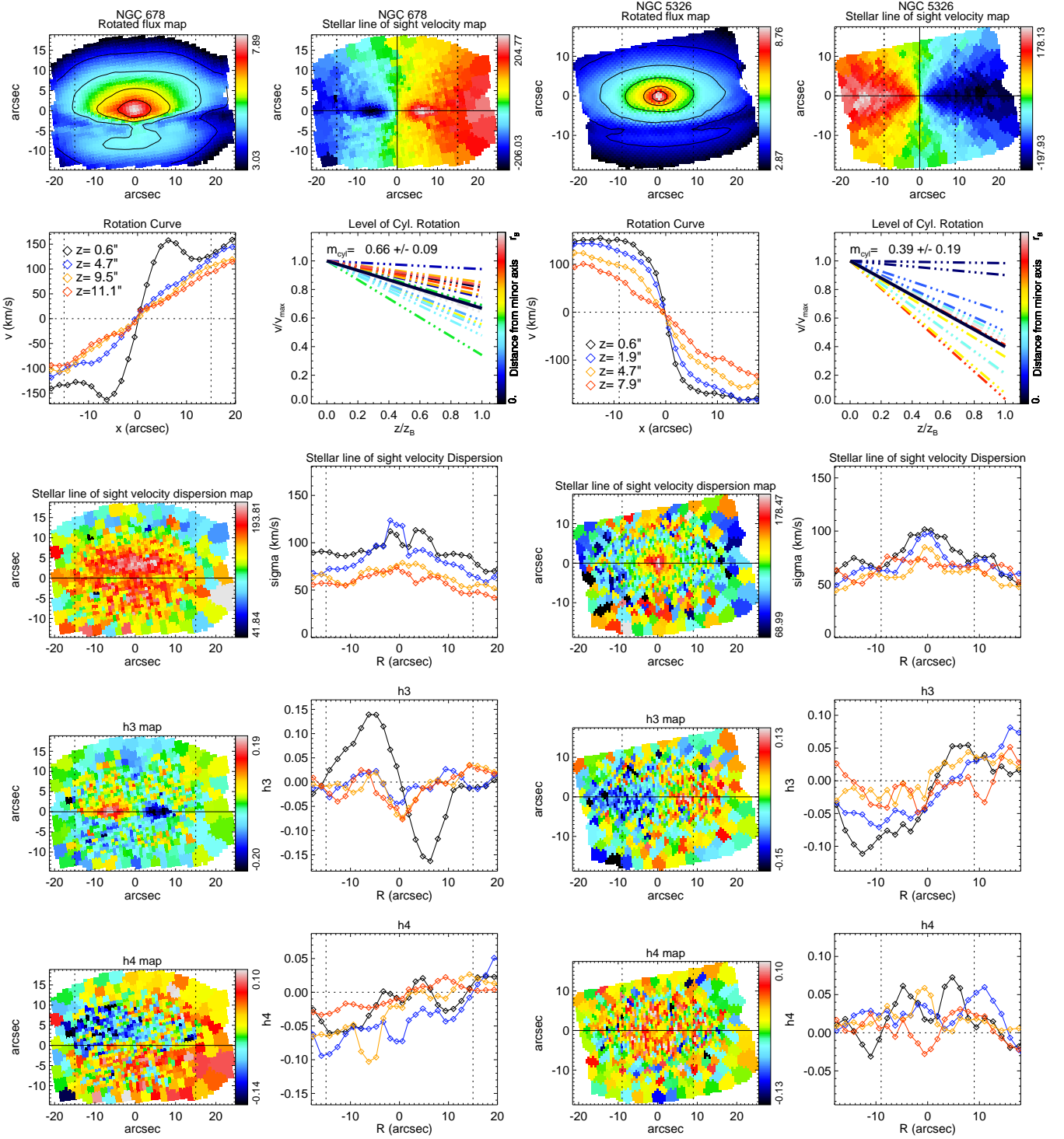


**Figure A2.** Sauron stellar kinematics maps, related profiles along cuts parallel to the major axis at four representative different heights from the disk plane and degree of cyl. rotation ( $m_{cyl}$ ) plot. The vertical dashed lines show the bulge boundary in  $r$  direction. Note that, all maps are rotated so that the for each galaxy the x axis are along the major axis of galaxy.



## NGC 5422

## NGC 5475

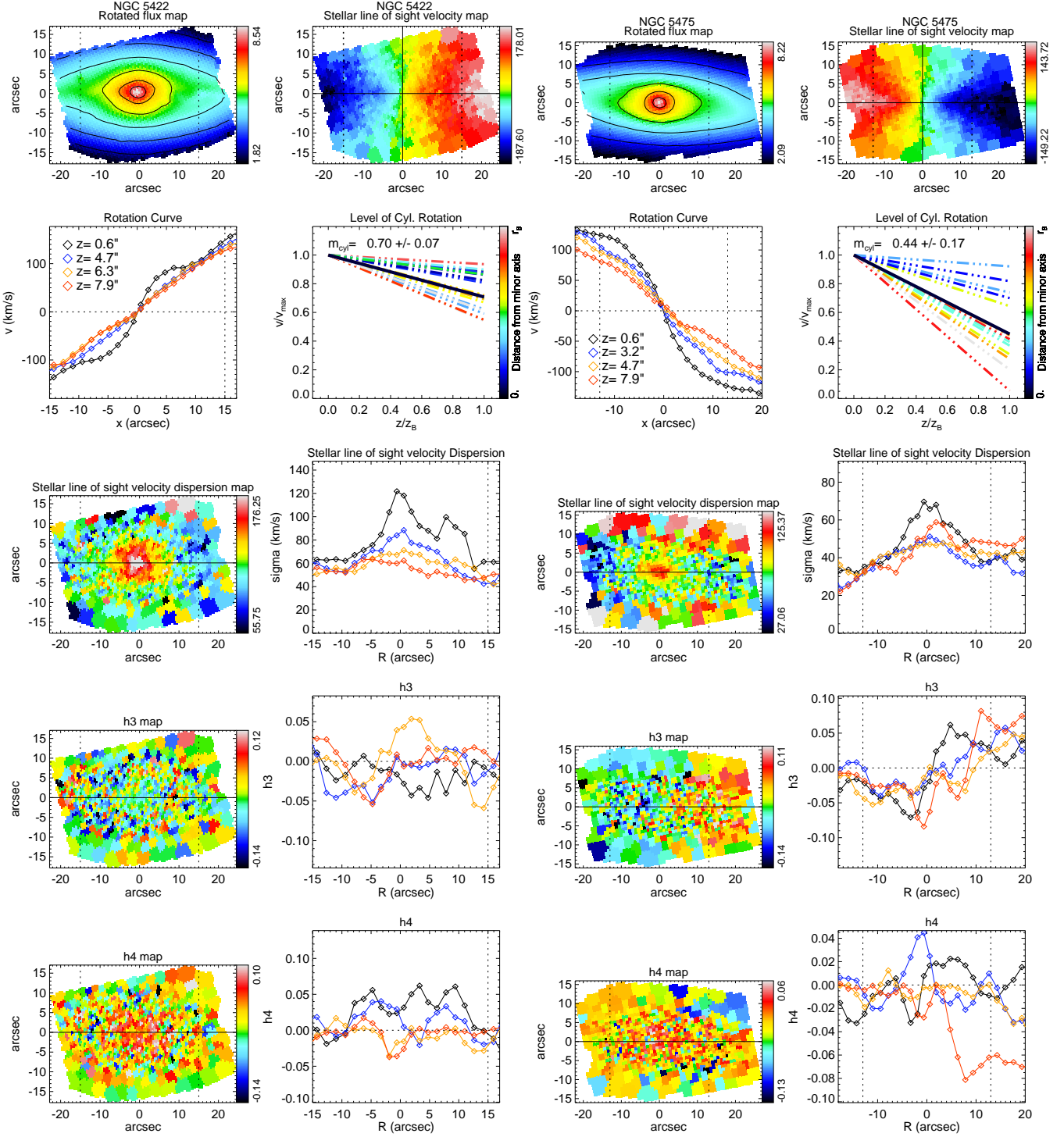


Figure A2. continued

## NGC 5689

## NGC 5707

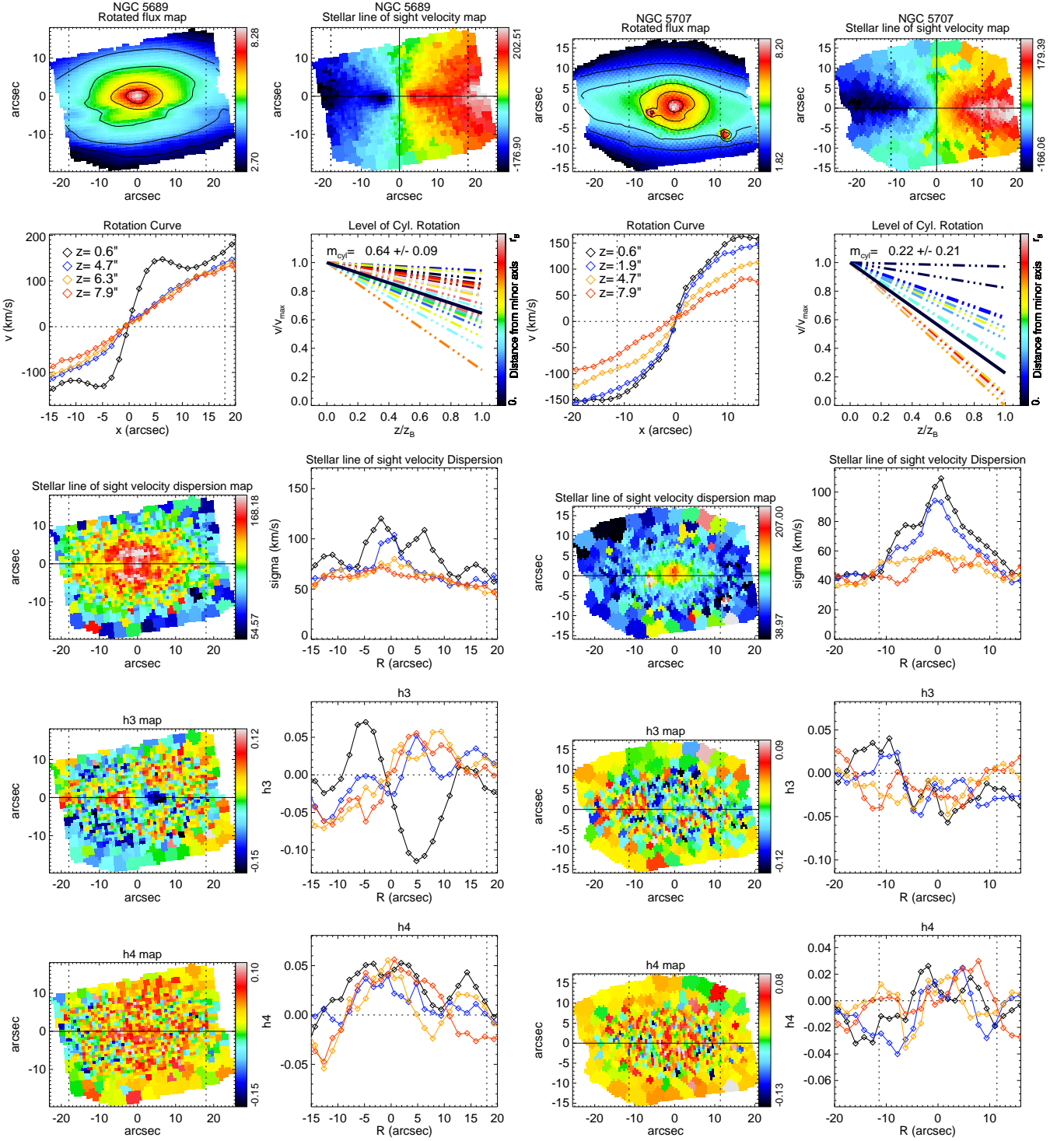


Figure A2. continued

## NGC 5746

## NGC 5838

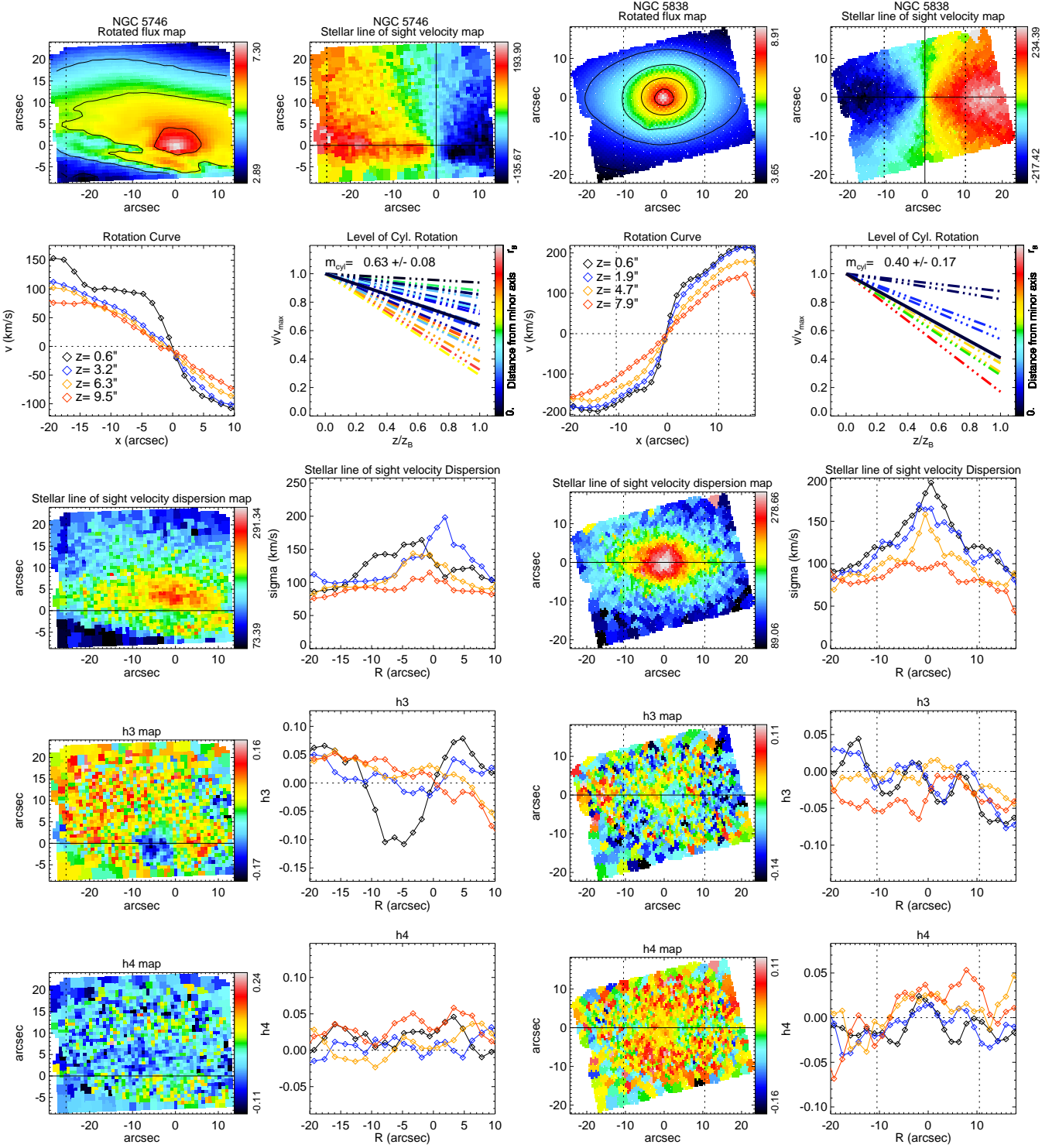


Figure A2. continued



## NGC 5965

## NGC 6010

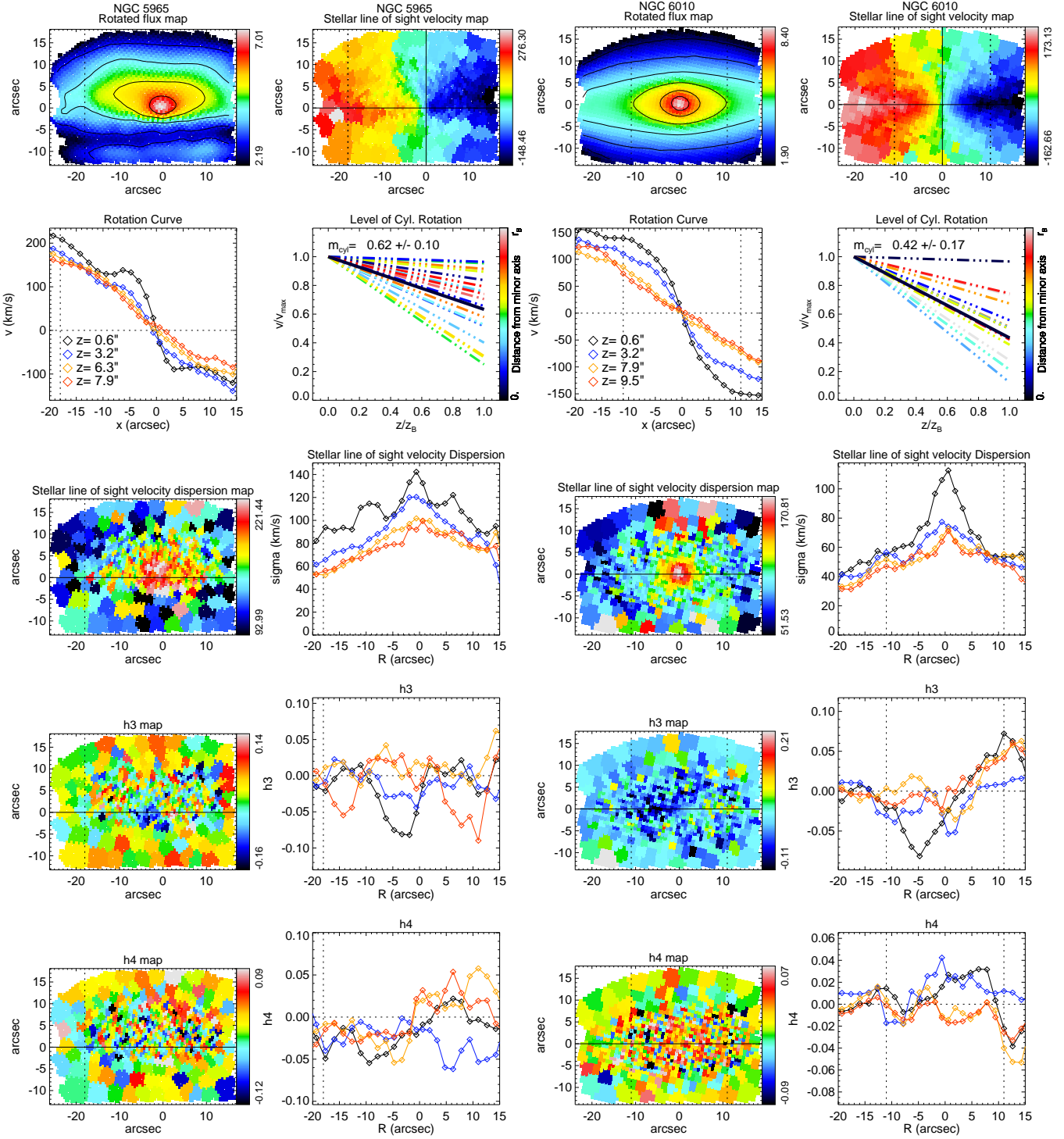


Figure A2. continued

## NGC 7332

## NGC 7457

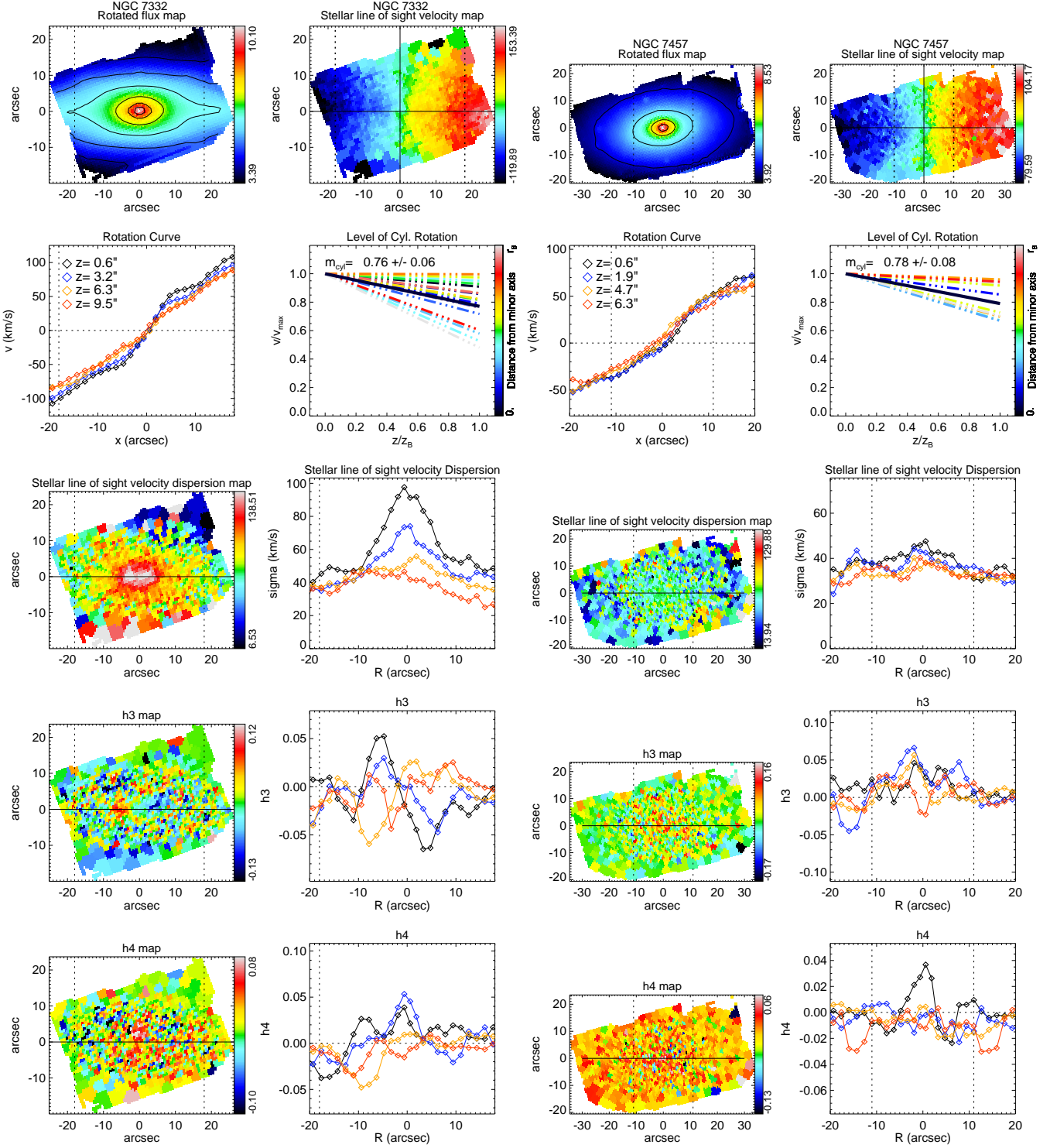


Figure A2. continued